CHAPTER IV

RESULTS AND DISCUSSION

4.1 Gas chromatographic separation of styrene oxide derivatives

Separations of all analytes were performed isothermally, at least in duplicate, in the temperature range of 40–200 °C at 10 °C intervals on three columns: OV-1701, GSiMe and GSiAc. The retention factor (k′) and enantioselectivity (α) of racemic aromatic epoxides at 120 °C are compared and shown in Figures 4.1–4.3.

Retention factor of the more retained enantiomer (k'_2) of aromatic epoxides on two chiral columns at 120 °C varied significantly in the range of 1.2–49.1 depending on type and number of substituents. All epoxides displayed higher retention on the two chiral columns, GSiMe and GSiAc, than on the nonchiral column OV-1701, even though all three columns have identical film thickness and contain polysiloxane OV-1701 as a major component of the stationary phase. This suggested that cyclodextrin derivatives were responsible for increased retention.

All racemic aromatic epoxides could be resolved into their enantiomers on at least one chiral column. The enantioselectivities of epoxides on two chiral columns at 120 °C are compared in Figure 4.4. Different trends were detected and the enantioselectivity values varied depending on type, number, and position of substituents. In most cases, the GSiAc column provided better enantioselectivity towards aromatic epoxides than did the GSiMe column. Nonetheless, due to the physical properties of analytes, such as boiling point and vapor pressure, are substantially different, retention factors and enantioselectivities at a specific temperature could not be directly compared. Therefore, thermodynamic parameters over a temperature range were determined to provide better understanding of the interactions between analytes and stationary phases.

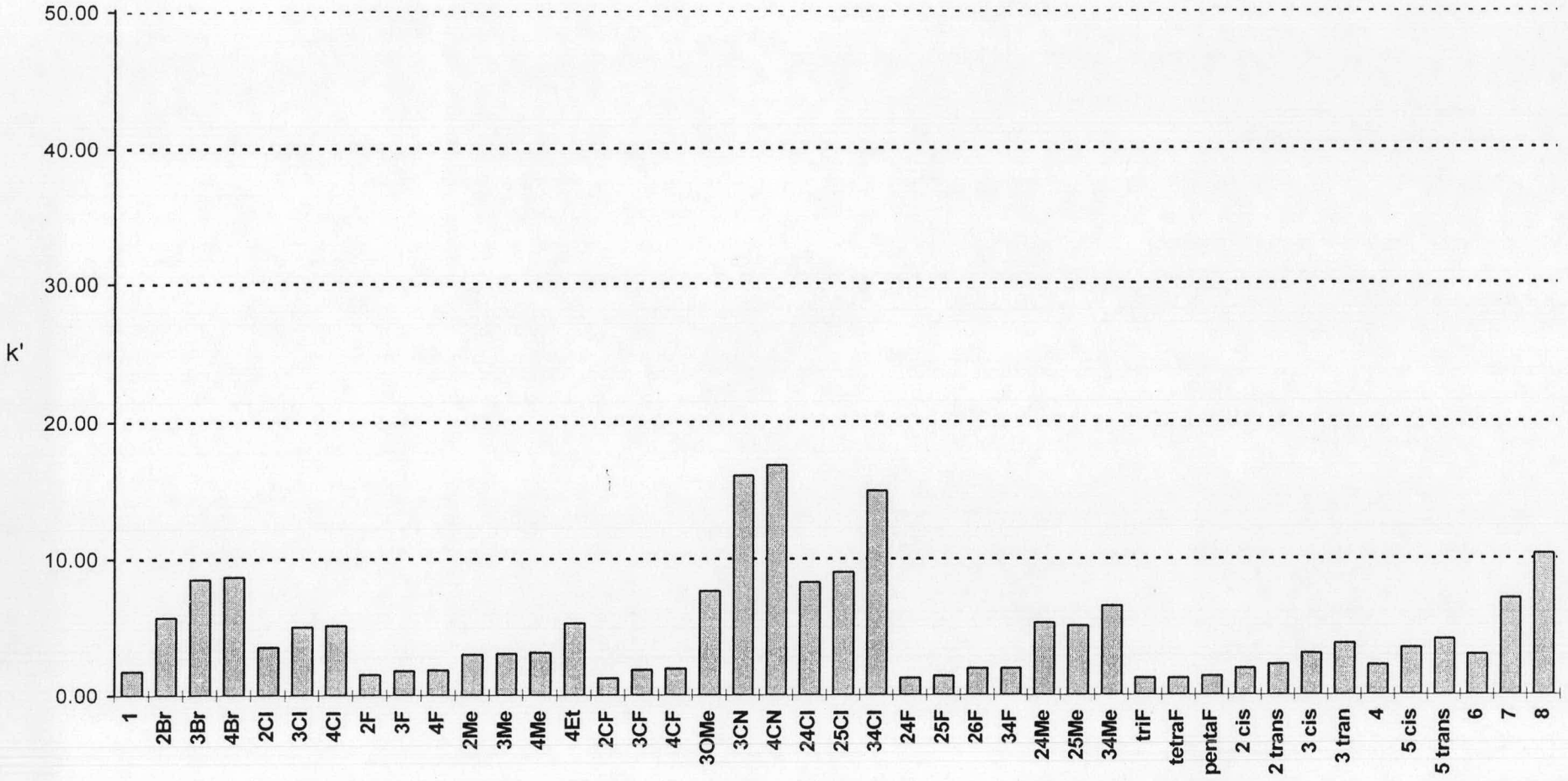

Figure 4.1 Retention factor (k′) of styrene oxide derivatives on OV-1701 column at 120 °C. See Table 3.1 for the analyte abbreviations.

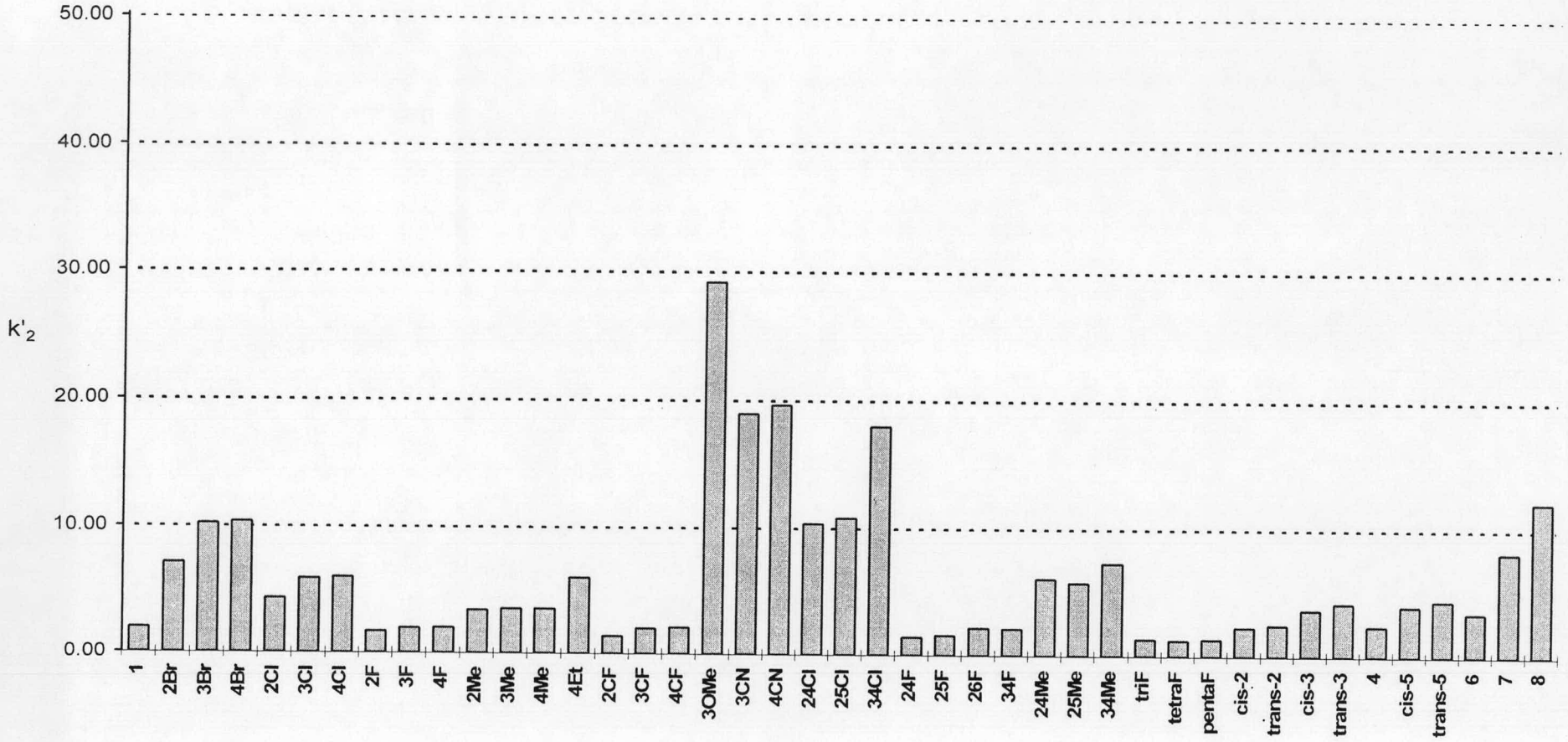

Figure 4.2 Retention factor (k'_2) of the more retained enantiomers of styrene oxide derivatives on GSiMe column at 120 °C. See Table 3.1 for the analyte abbreviations.

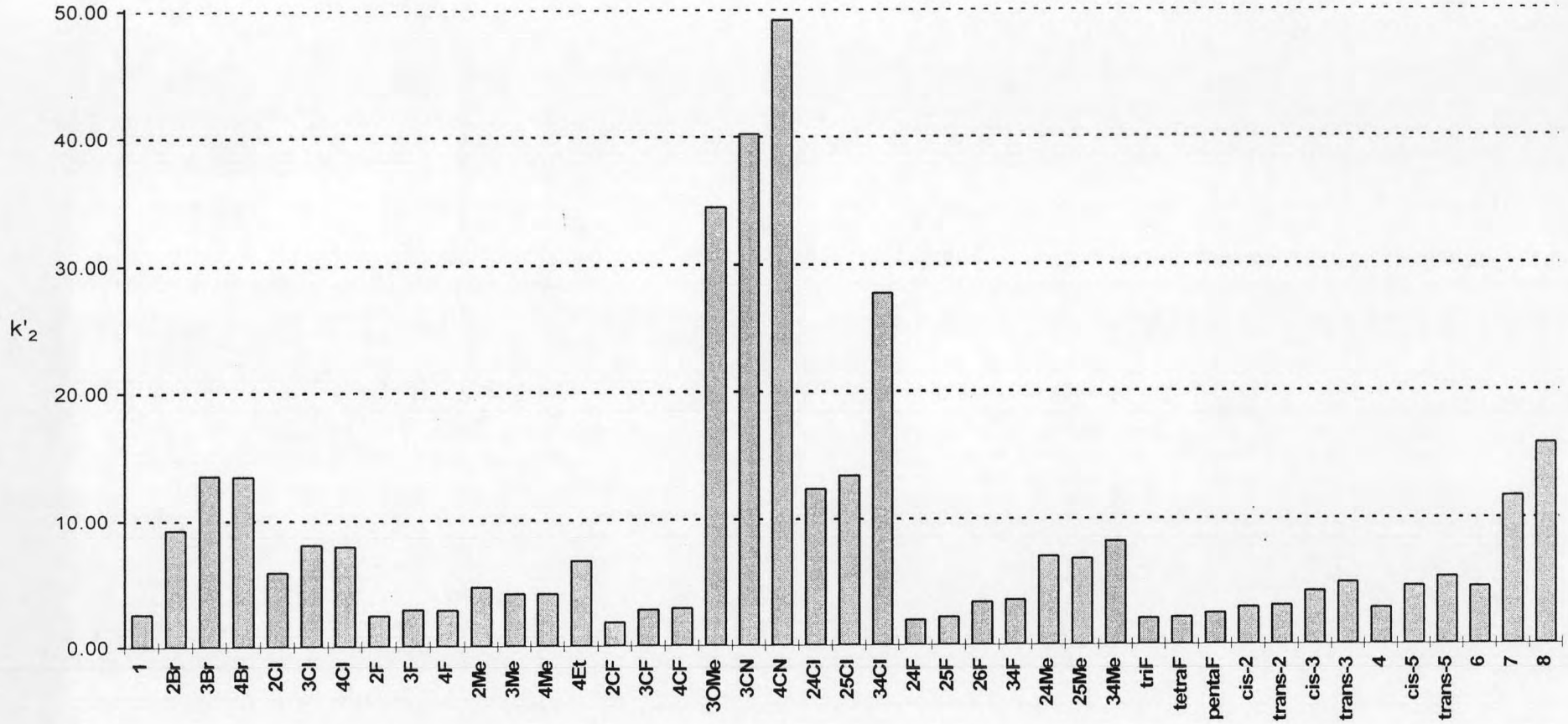

Figure 4.3 Retention factor (k'_2) of the more retained enantiomers of styrene oxide derivatives on GSiAc column at 120 °C. See Table 3.1 for the analyte abbreviations.

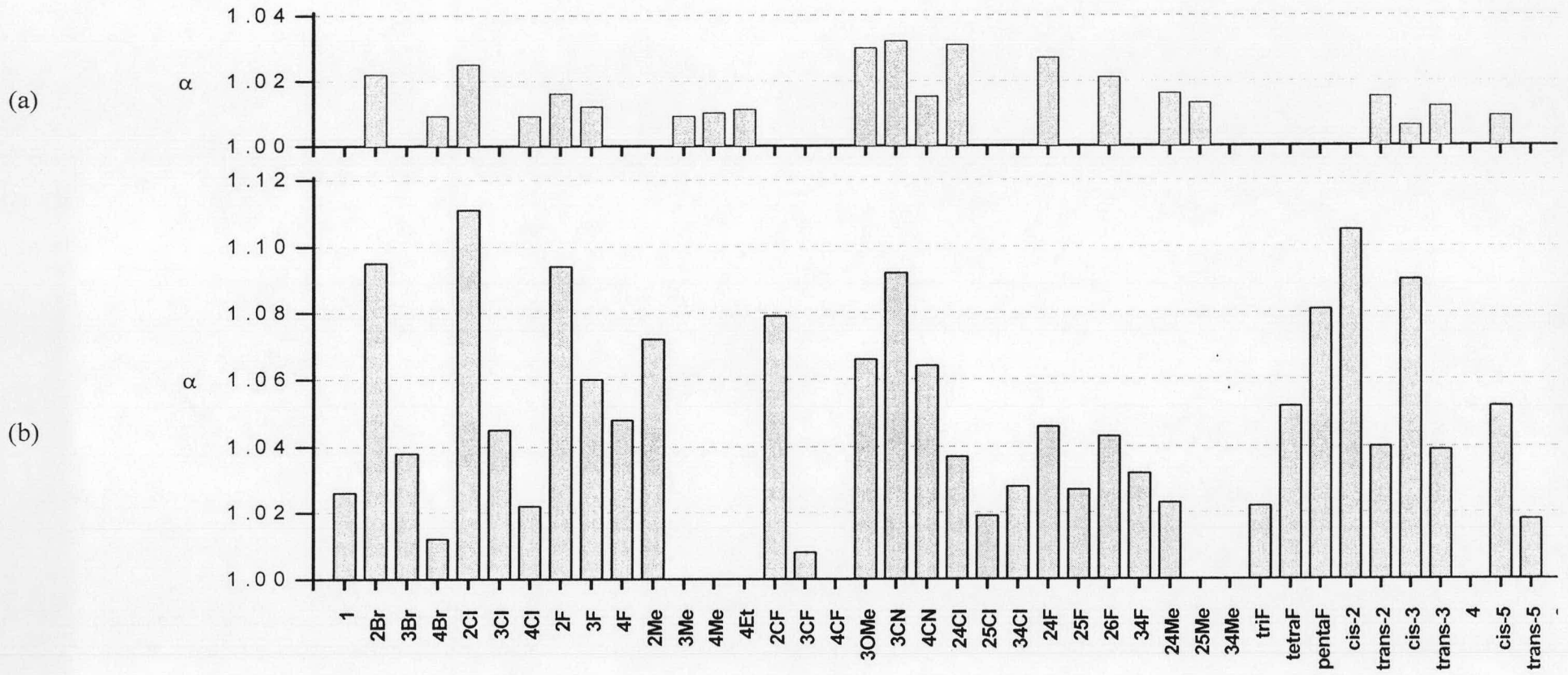

Figure 4.4 Separation factor (α) of the enantiomeric pairs of styrene oxide derivatives on (a) GSiMe and (b) GSiAc columns at 120 °C. See Table 3.1 for the analyte abbreviations.

4.2 Thermodynamic investigation by van't Hoff approach

Thermodynamic parameters associated with the interactions between chiral epoxides and stationary phase could be acquired through the van't Hoff plot (see equation (7) in section 2.4). All ln k′ versus 1/T plots showed linear relationship with correlation coefficient value (R^2) greater than 0.9988. From these plots, enthalpy (ΔH) and entropy (ΔS) values for each enantiomer could be calculated from slope and y-intercept, respectively. When enantiomeric pairs were separated, the enthalpy and entropy differences ($\Delta\Delta H$ and $\Delta\Delta S$, respectively) could be determined from the relationship between ln α and 1/T. Theoretically, the ln α and 1/T plot should be linear; however, nonlinear plots are occasionally observed in the temperature range studied. Alternatively, the $\Delta\Delta H$ and $\Delta\Delta S$ values can also be calculated from the differences in ΔH and ΔS values of two enantiomers. As a result, the $\Delta\Delta H$ and $\Delta\Delta S$ values obtained from the latter approach were presented in this study.

4.2.1 Enthalpy change (ΔH) and entropy change (ΔS)

Enthalpy change (ΔH) indicates the strength of interaction between the analyte and stationary phase: the larger the enthalpy change (more negative value), the higher the strength of interaction. Entropy change (ΔS) indicates the loss of degree of freedom resulted from the interaction between enantiomer and stationary phase.

The $-\Delta H$ values of most epoxides on the OV-1701 reference column were very similar (Figure 4.5). In addition, aromatic (**1**) and aliphatic (**octa**) epoxides with the same number of carbons give similar $-\Delta H$ values. This suggests that major contribution from analytes towards the interaction comes from the epoxy group. Aromatic epoxides with cyano or nitro group tend to exhibit stronger interaction than do the other compounds. On the contrary, the $-\Delta H$ values of aliphatic epoxides tend to increase with the chain length. A similar trend is observed for the $-\Delta S$ values (Figure 4.6)

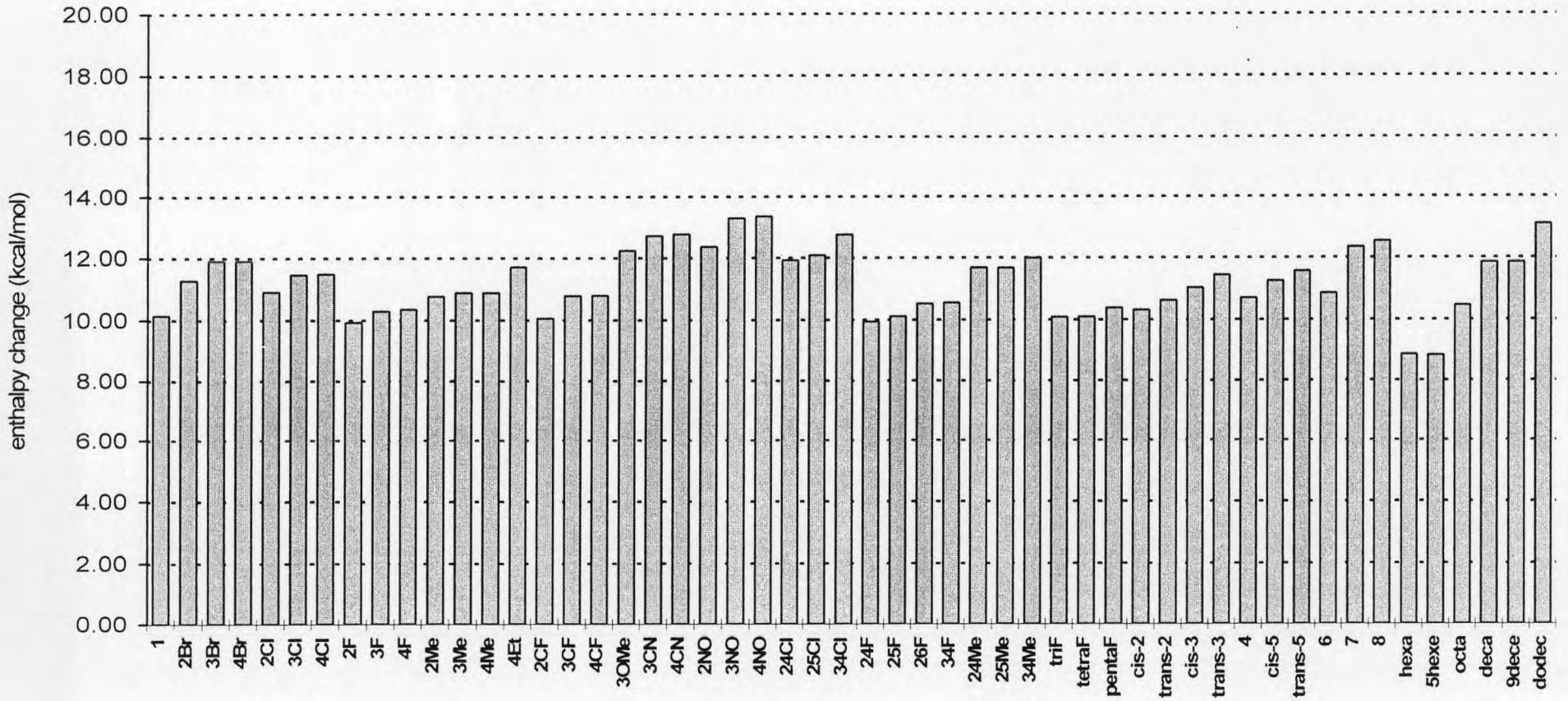

Figure 4.5 Enthalpy change (−ΔH, kcal/mol) of epoxide analytes on OV-1701 column obtained from van't Hoff approach ($\bar{x}$ = 11.22; SD = 1.05). See Table 3.1 for the analyte abbreviations.

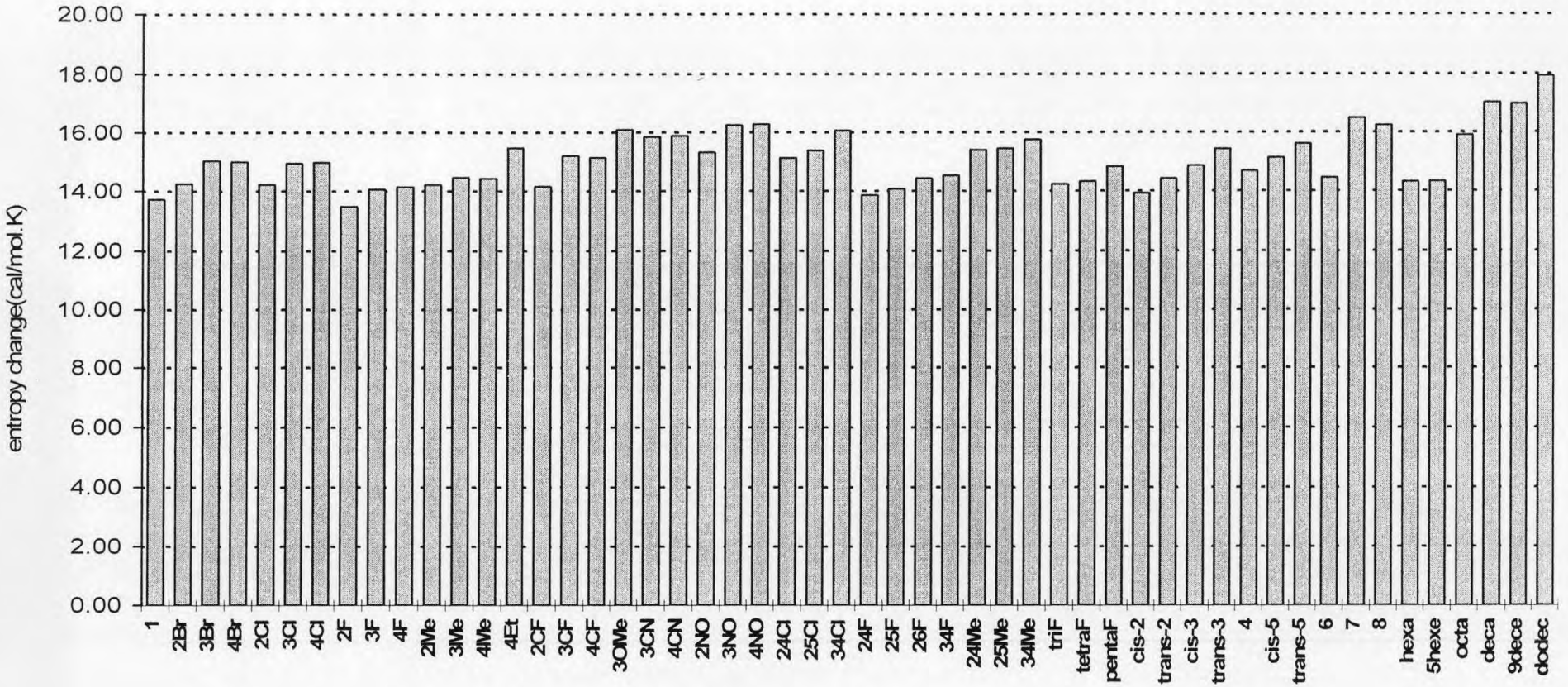

Figure 4.6 Entropy change (−ΔS, cal/mol·K) of epoxide analytes on OV-1701 column obtained from van't Hoff approach ($\bar{x}$ = 15.06; SD = 0.94). See Table 3.1 for the analyte abbreviations.

Enthalpy and entropy values of the more retained enantiomers ($-\Delta H_2$ and $-\Delta S_2$) of epoxides on GSiMe (Figures 4.7 and 4.8) and GSiAc (Figures 4.9 and 4.10) columns were higher than those on OV-1701 column (Figures 4.5 and 4.6) indicating the stronger interaction between analytes and cyclodextrin derivatives. The average enthalpy ($-\Delta H_2$) and entropy ($-\Delta S_2$) values attained from GSiAc column (-13.16 ± 1.36 and -19.10 ± 1.67, respectively) were a little higher than those from GSiMe column (-12.31 ± 1.17 and -17.57 ± 1.22, respectively). The stronger interaction between GSiAc and epoxides would come from polar acetyl groups of cyclodextrin. However, most epoxides interact with stationary phase similarly as their enthalpy and entropy values on the same column were not significantly different. The $-\Delta H_2$ and $-\Delta S_2$ values of isomers of mono-substituted aromatic epoxides on GSiMe slightly decrease in the order of *para-* > *meta-* > *ortho-*, whereas values on GSiAc are not significantly different.

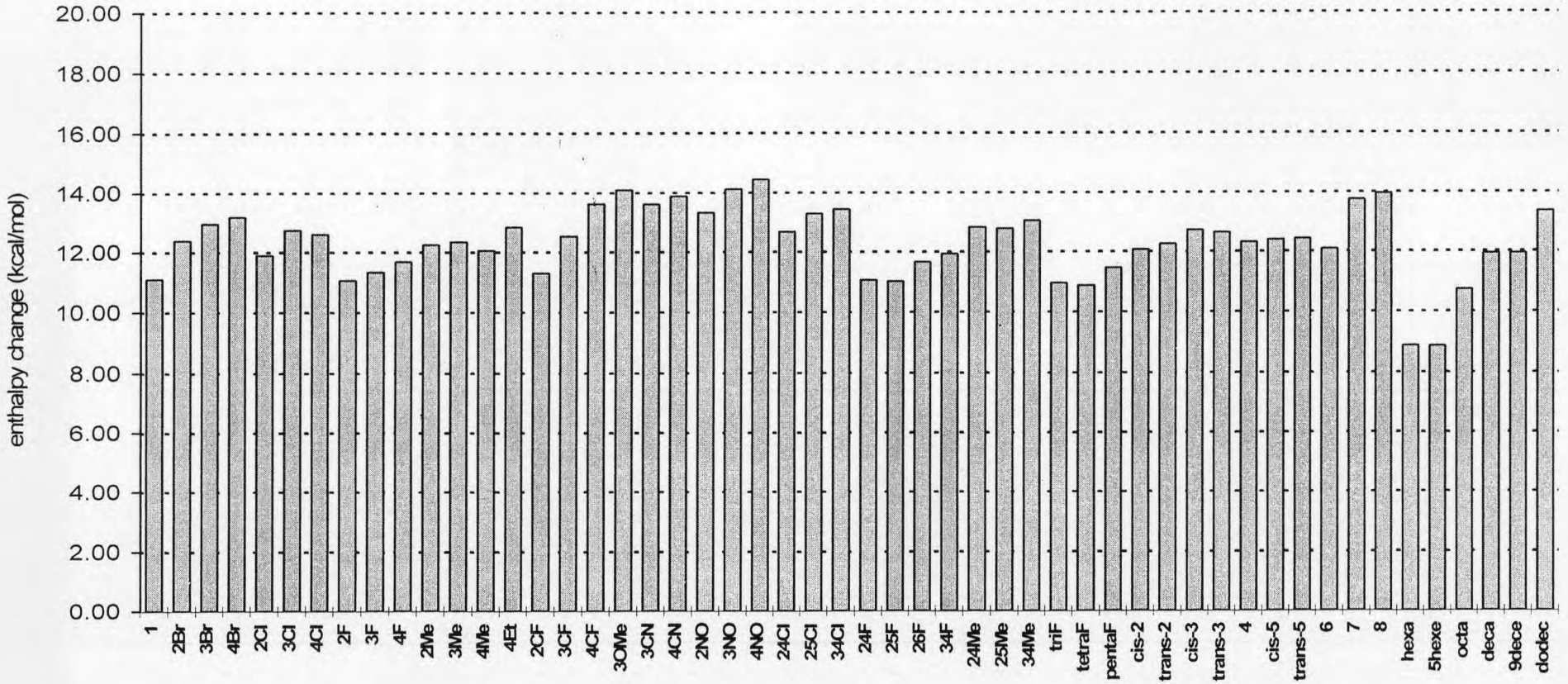

Figure 4.7 Enthalpy change ($-\Delta H_2$, kcal/mol) of the more retained enantiomers of epoxide analytes on GSiMe column obtained from van't Hoff approach ($\bar{x}$ = 12.31; SD = 1.17). See Table 3.1 for the analyte abbreviations.

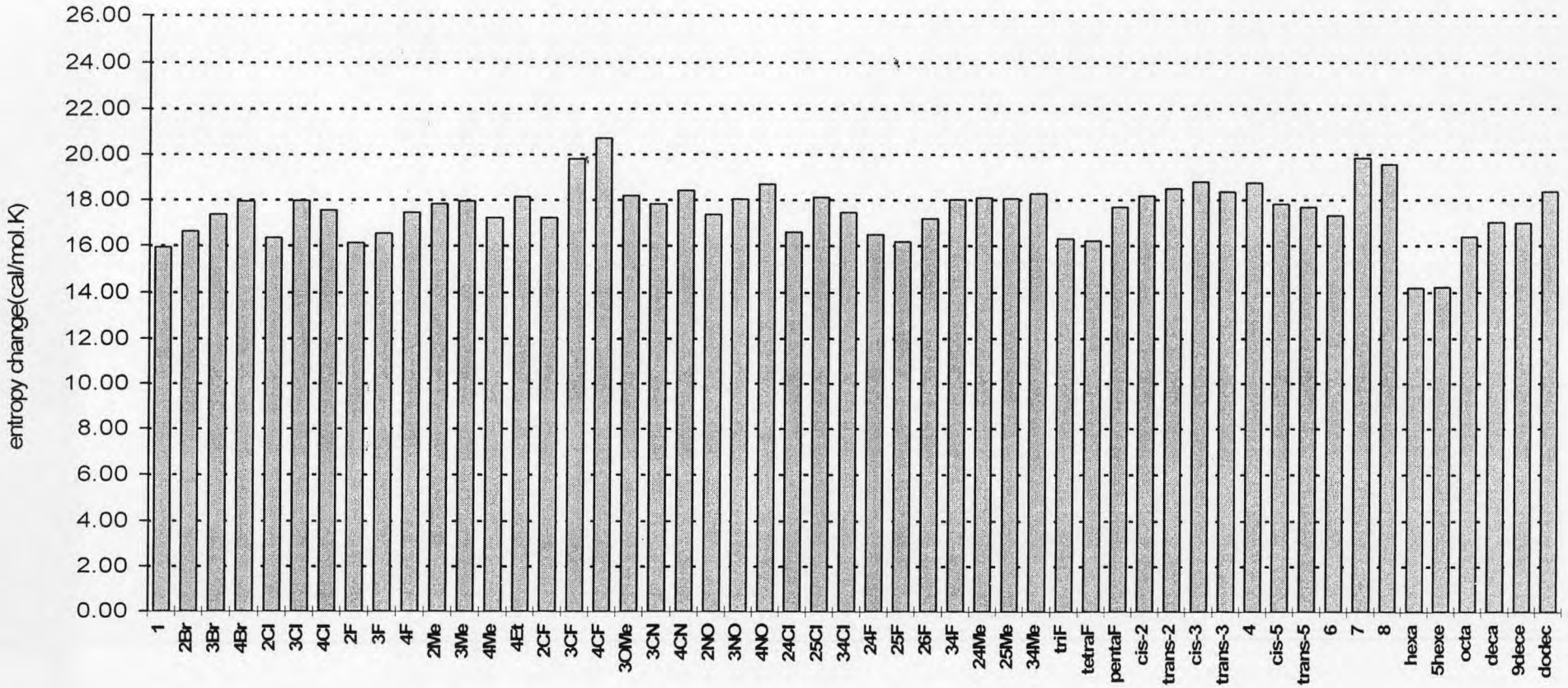

Figure 4.8 Entropy change ($-\Delta S_2$, cal/mol·K) of the more retained enantiomers of epoxide analytes on GSiMe column obtained from van't Hoff approach ($\bar{x}$ = 17.57; SD = 1.22). See Table 3.1 for the analyte abbreviations.

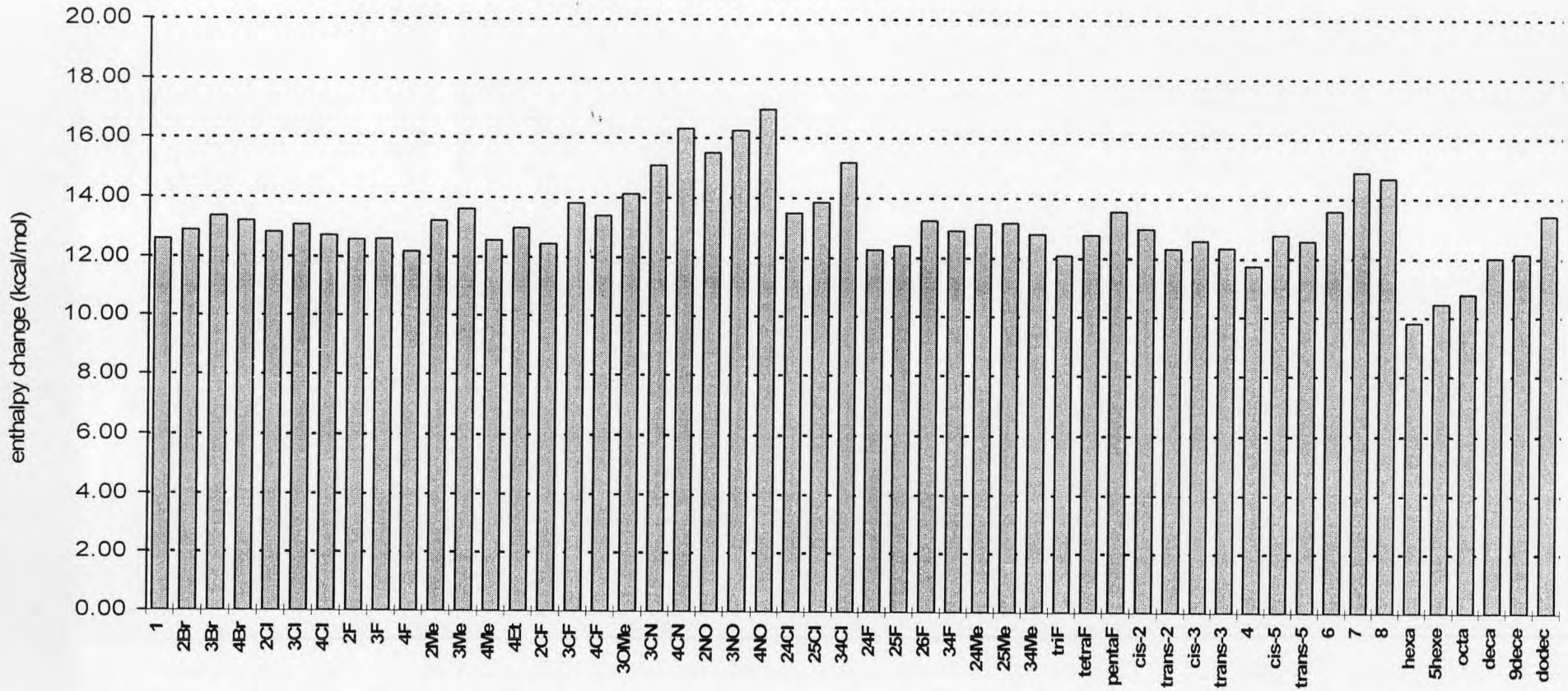

Figure 4.9 Enthalpy change ($-\Delta H_2$, kcal/mol) of the more retained enantiomers of epoxide analytes on GSiAc column obtained from van't Hoff approach ($\bar{x}$ = 13.16; SD = 1.34). See Table 3.1 for the analyte abbreviations.

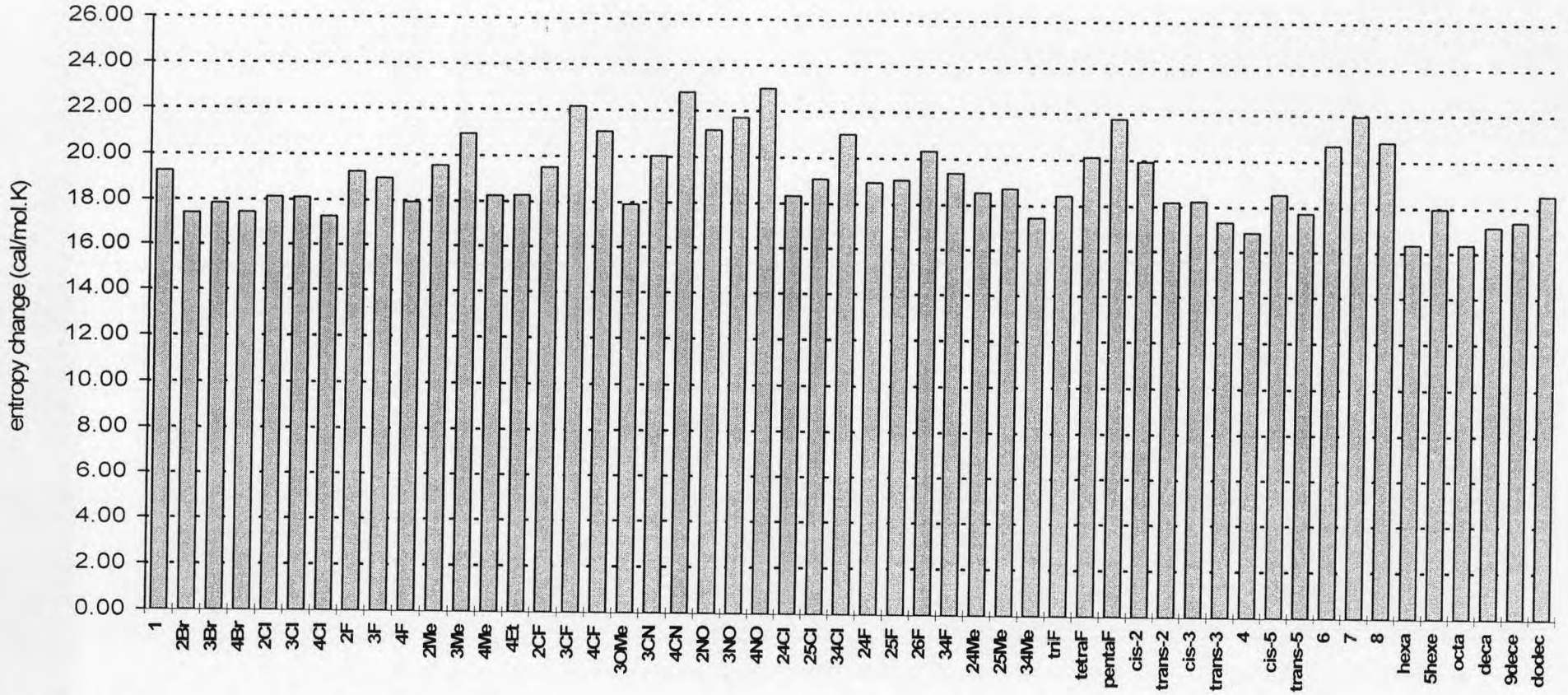

Figure 4.10 Entropy change ($-\Delta S_2$, cal/mol·K) of the more retained enantiomers of epoxide analytes on GSiAc column obtained from van't Hoff approach ($\bar{x}$ = 19.10; SD = 1.67). See Table 3.1 for the analyte abbreviations.

4.2.2 Enthalpy difference (−ΔΔH) and entropy difference (−ΔΔS)

In this research, styrene oxide (**1**) was regarded as a reference analyte and the influence of analyte structure and substituents on enantioseparation were systematically examined and discussed through the thermodynamic values. The −ΔΔH and −ΔΔS values shown in this research derived from the difference in −ΔH and −ΔS of enantiomeric pairs through van't Hoff plot of ln k′ versus 1/T. The −ΔΔH and −ΔΔS values of all analytes on GSiMe and GSiAc columns were exhibited in Figures 4.11 and 4.12. In general, the GSiAc column shows better enantioseparation (higher −ΔΔH and −ΔΔS values) towards most epoxides than does the GSiMe column. The −ΔΔS values of analytes on both columns displayed similar trend as their corresponding −ΔΔH values. Therefore, enantioseparation will be discussed through −ΔΔH values only. The −ΔΔH values of all analytes were significantly different depending on analyte structure, i.e. type, position, and number of substituents. The influence of analyte structure on enantioseparation will be discussed and classified into four groups according to the similarity of analyte structure.

(a)

(b)

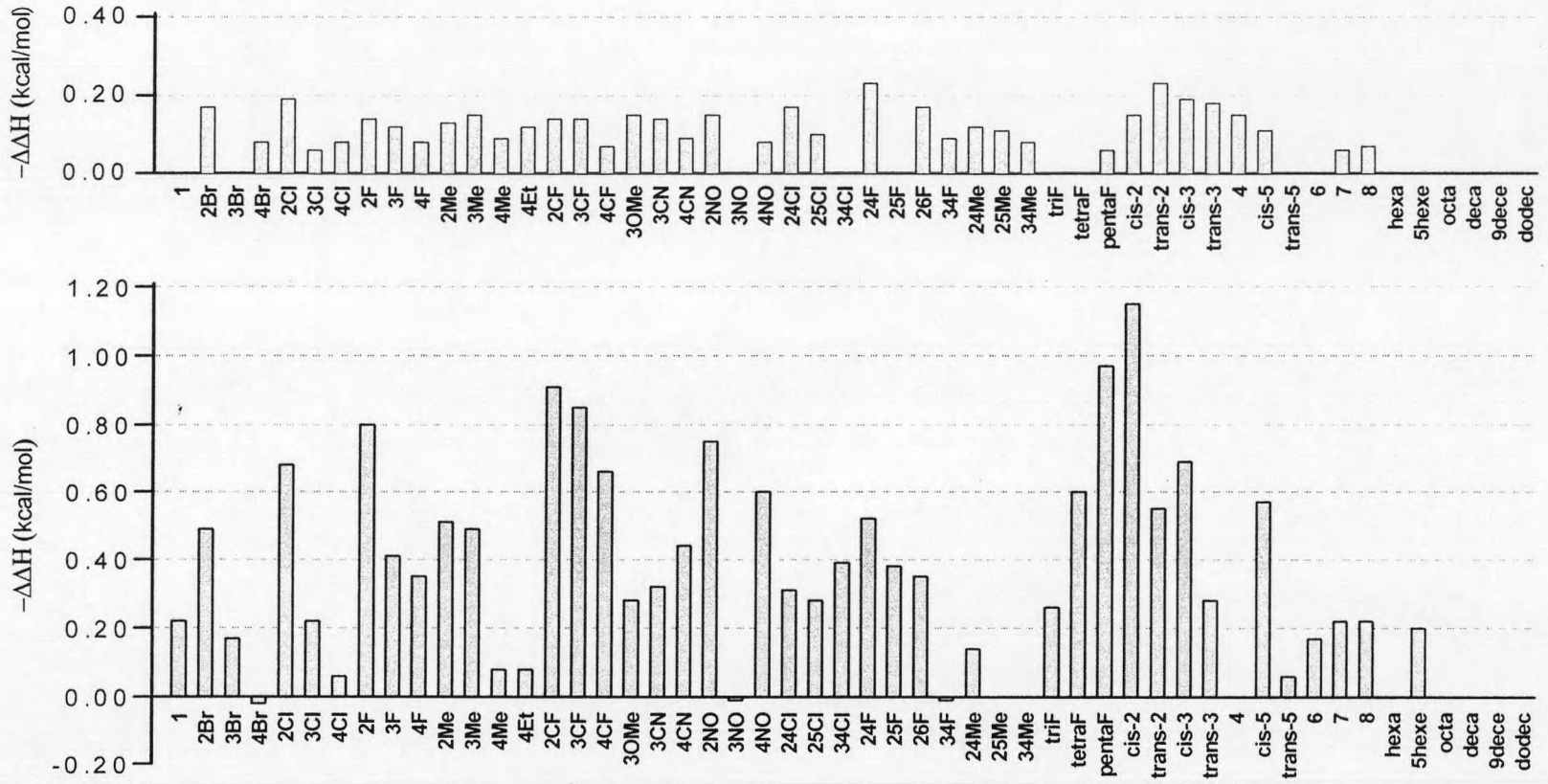

Figure 4.11 Enthalpy difference, −ΔΔH (kcal/mol) of the enantiomers of epoxide analytes on (a) GSiMe and (b) GSiAc columns. See Table 3.1 for the analyte abbreviations.

(a)

(b)

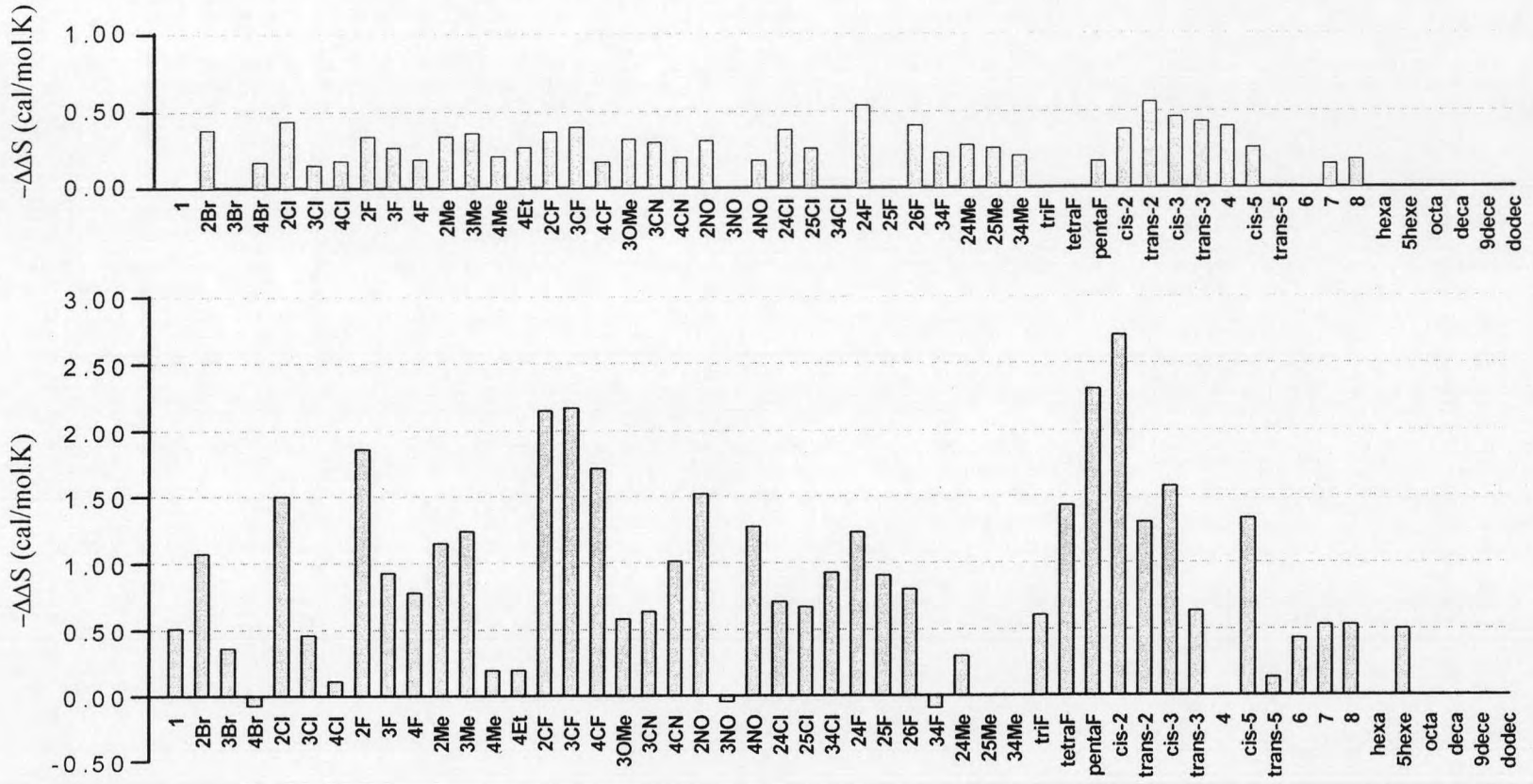

Figure 4.12 Entropy difference, −ΔΔS (cal/mol·K) of the enantiomers of epoxide analytes on (a) GSiMe and (b) GSiAc columns. See Table 3.1 for the analyte abbreviations.

Group 1: Styrene oxides with mono-substitution on the aromatic ring

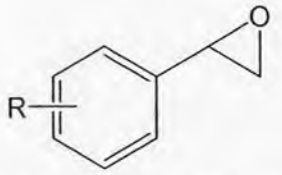

R = Br, Cl, F, CH_3, C_2H_5, OCH_3, CN, NO_2, CF_3

Racemic epoxides in group 1 are styrene oxide derivatives with mono-substitution on the aromatic ring as shown above. The substituent type includes bromo, chloro, fluoro, methyl, ethyl, methoxy, cyano, nitro, and trifluoromethyl at *ortho*-, *meta*- and *para*-positions. The $-\Delta\Delta H$ values representing enantioseparation of epoxides in group 1 on GSiMe and GSiAc columns are displayed in Figures 4.13 and 4.14, respectively.

On the GSiMe column, the $-\Delta\Delta H$ values of all analytes are rather small (Figure 4.13). However, the position of substitution plays an important role in enantioseparation than does the type of substitution. While a reference analyte, styrene oxide (**1**), showed no enantioseparation, *ortho*-substituted styrene oxides displayed high $-\Delta\Delta H$ values. *Meta*- and *para*-substituted styrene oxides have lower $-\Delta\Delta H$ values than *ortho*-substituted analytes. Unfortunately, GSiMe gave no enantioseparation towards bromo- and nitro-substituted styrene oxides at *meta*-position. Among six *ortho*-substituted analytes, **2Cl** exhibited the highest $-\Delta\Delta H$ value and gave the best separation. The $-\Delta\Delta H$ values of chloro-substituted styrene oxides decreased in order of **2Cl** > **4Cl** > **3Cl**. The relationship between ln α and 1/T of three chloro-substituted styrene oxides are shown in Figure 4.15. It is clear that **2Cl** has the highest enantioselectivity (α) at all temperatures. Furthermore, **2Cl** also has the highest slope, indicating that the enantioseparation of **2Cl** could be easily increased with a slight decrease in temperature. The separations of **2Cl**, **3Cl**, and **4Cl** at 110 °C are shown in Figure 4.16.

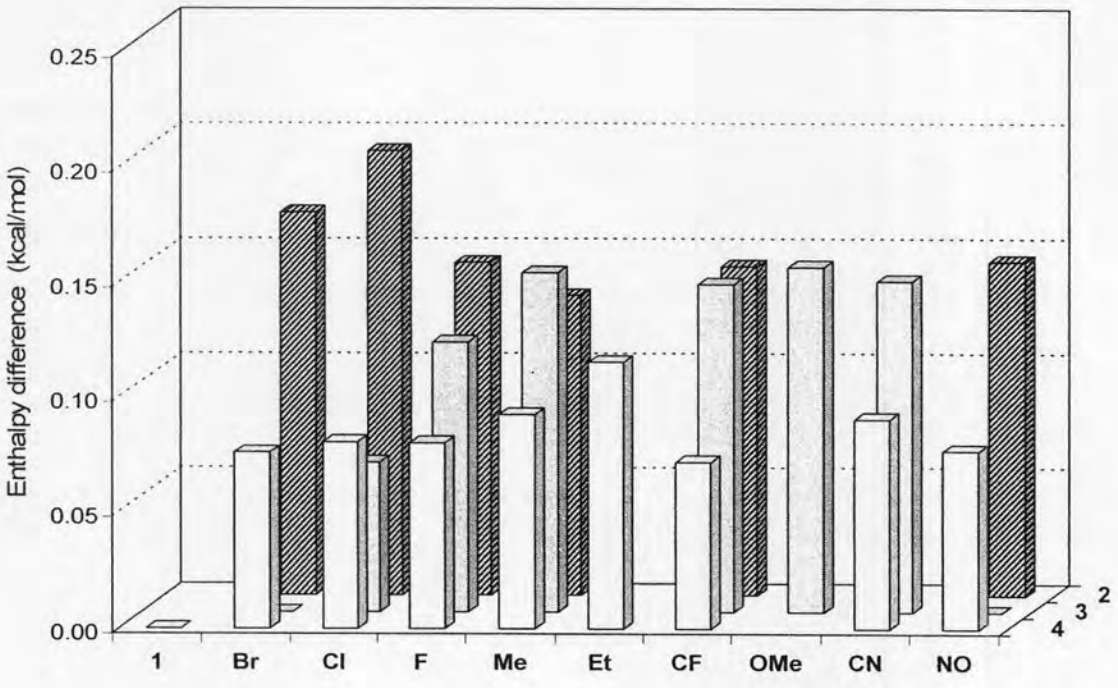

Figure 4.13 Enthalpy difference, −ΔΔH (kcal/mol) of the enantiomers of mono-substituted styrene oxides on GSiMe column.

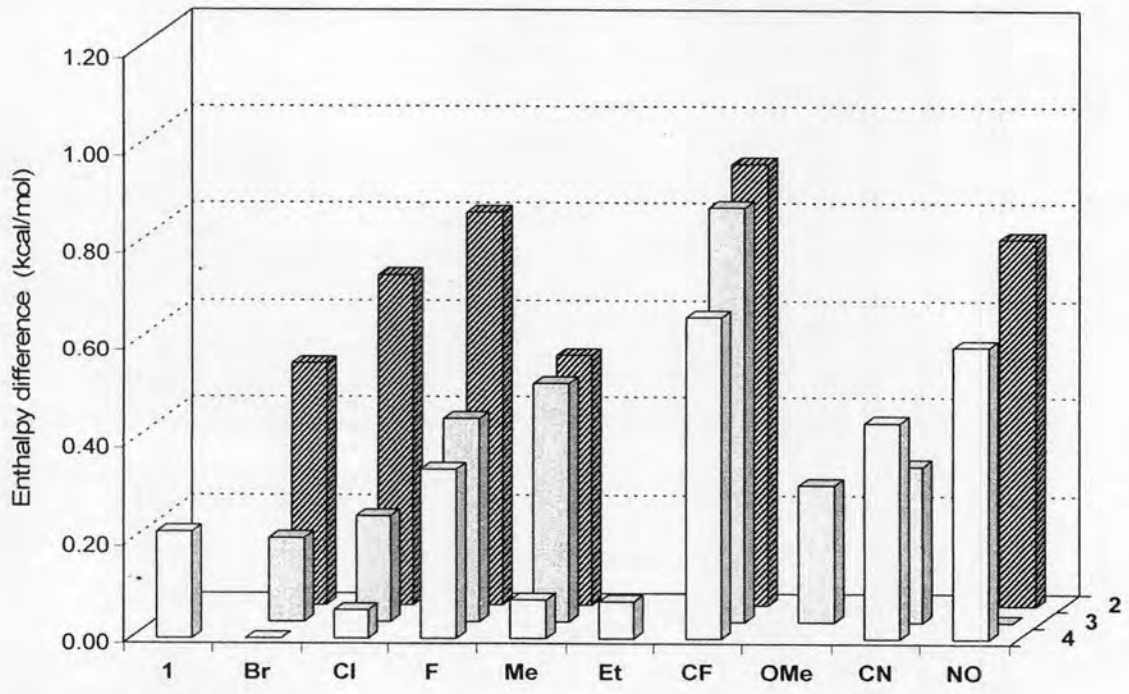

Figure 4.14 Enthalpy difference, −ΔΔH (kcal/mol) of the enantiomers of mono-substituted styrene oxides on GSiAc column.

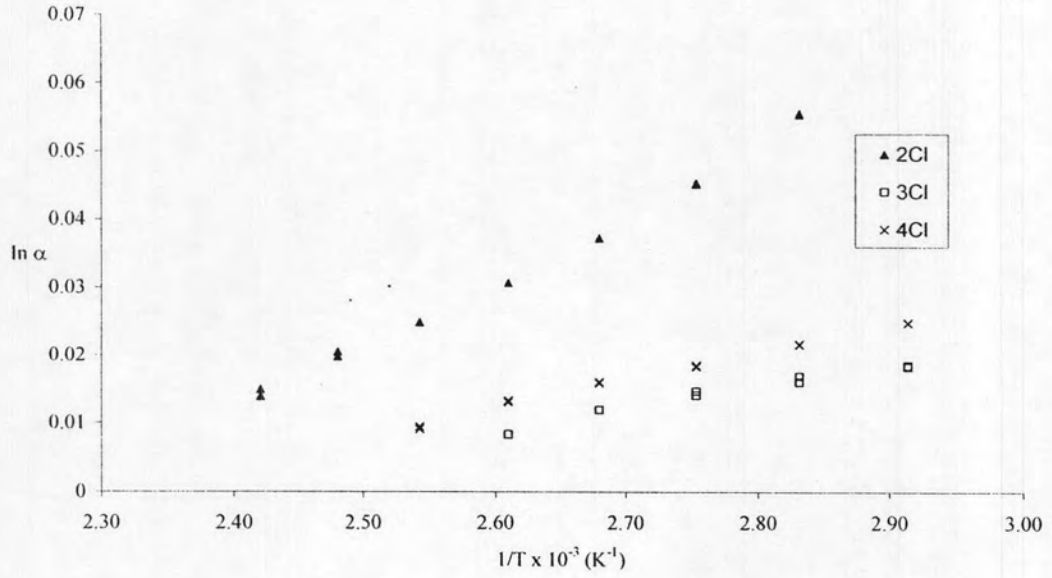

Figure 4.15 Plots of ln α versus 1/T of **2Cl**, **3Cl**, and **4Cl** on GSiMe column.

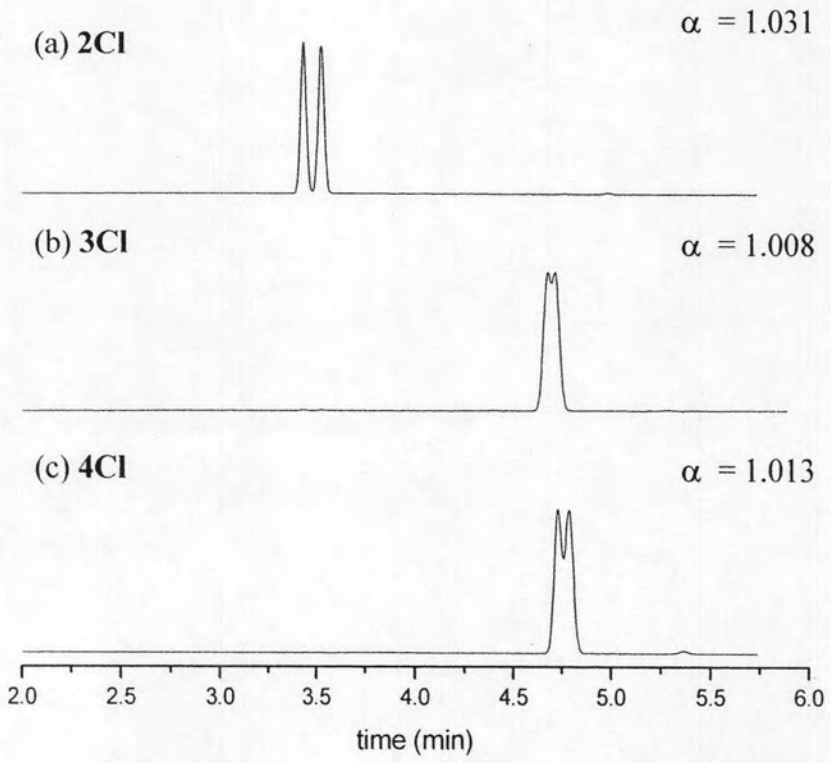

Figure 4.16 Chromatograms of (a) **2Cl**, (b) **3Cl**, and (c) **4Cl** on GSiMe column at 110 °C.

Enantioseparation of mono-substituted styrene oxides on GSiAc column, where cyclodextrin substituents were changed from nonpolar methyl to polar acetyl groups (Figure 4.14). The $-\Delta\Delta H$ values from GSiAc column were much larger than those obtained from GSiMe column (Figure 4.13 and 4.14). Considering the effect of substituent position, *ortho*-position on the aromatic ring seemed to promote enantiorecognition as seen from high $-\Delta\Delta H$ values. The $-\Delta\Delta H$ values of substituted analytes are in order of *ortho-* > *meta-* > *para-*, except for cyano and nitro groups. While **1**, **3Br**, and **3NO** could not be separated on GSiMe, they showed separation on GSiAc. Furthermore, the effect of electronegative substituent on enantioseparation on GSiAc column was observed. The fluoro- and trifluoromethyl-substituted styrene oxides showed enhanced enantioseparation on GSiAc column. Among all analytes in group 1, **2CF** gave the best enantioseparation.

Note that both $-\Delta\Delta H$ and $-\Delta\Delta S$ values of **4Br** on GSiAc column are opposite to those on GSiMe column (Figures 4.11 and 4.12). A plot of ln α versus 1/T of **4Br** on GSiAc column exhibits a separation selectivity maximum (Figure 4.17). It is likely that **4Br** interacts with GSiAc by multiple interaction mechanisms in this temperature range [44].

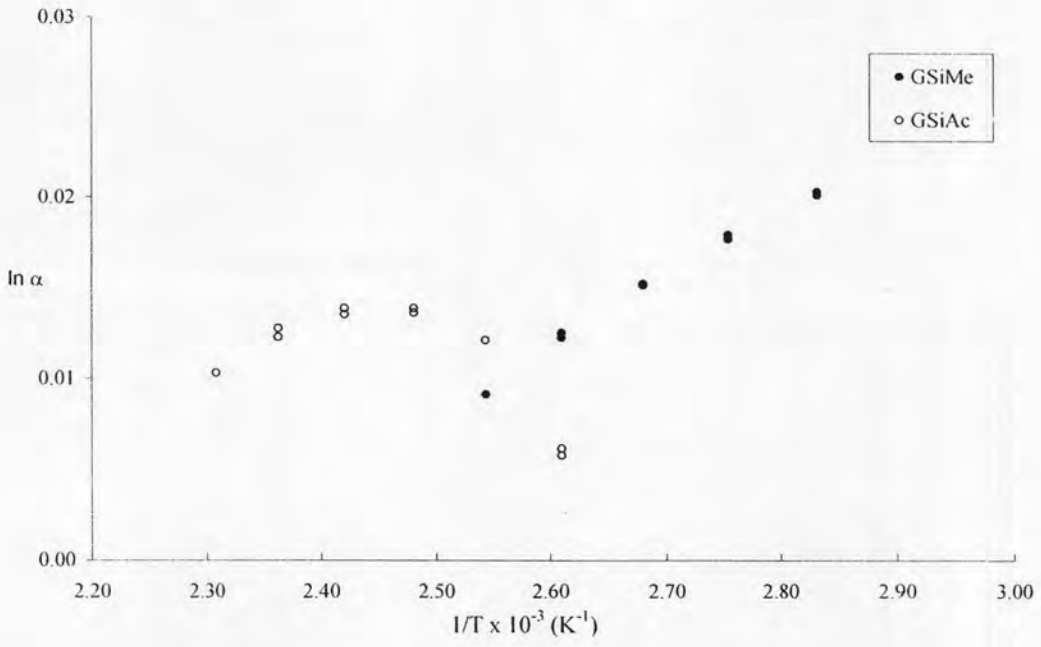

Figure 4.17 Plots of ln α versus 1/T of **4Br** on GSiMe and GSiAc columns.

The average $-\Delta\Delta H$ values of epoxides in group 1 obtained from GSiMe and GSiAc columns were also compared to those from BSiMe and BSiAc columns [16]. It was found that the average $-\Delta\Delta H$ values increased in order of GSiMe < BSiAc < BSiMe < GSiAc. *Ortho*-substitution on the aromatic ring seemed to promote enantiorecognition as observed in GSiMe, GSiAc as well as BSiMe columns. In addition, mono-substituted aromatic epoxides at *meta*- and *para*- positions that poorly or could not be separated on GSiAc column were well resolved on BSiMe or BSiAc column. This indicates that the size and substituent of cyclodextrin derivatives strongly affect enantioseparation.

Group 2: Styrene oxides with di-substitution on the aromatic ring

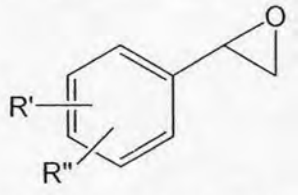

R′ = R″ = Cl, F, CH_3

Racemic epoxides in group 2 consist of styrene oxide derivatives with dichloro-, difluoro- and dimethyl-substituents at different position on the aromatic ring. The $-\Delta\Delta H$ values representing enantioseparation of enantiomers of epoxides in group 2 on GSiMe and GSiAc columns were shown in Figures 4.18 and 4.19, respectively.

For di-substituted styrene oxides, the trend of $-\Delta\Delta H$ values was not apparent as to those of mono-substituted derivatives since not all six isomers of each derivative were available. Position of substituent on the aromatic ring still played an important role in enantioseparation as styrene oxides with substituents at 2,4-position showed high $-\Delta\Delta H$ values (Figure 4.18). Among all 10 di-substituted analytes, **24F** displayed the highest $-\Delta\Delta H$ values on GSiMe. Nonetheless, **25F** and **34Cl** could not be separated on this column.

The $-\Delta\Delta H$ values of most di-substituted styrene oxides on GSiAc column were higher than those on GSiMe column demonstrating better enantioseparation. Analytes **25F** and **34Cl** in group 2 that could not be successfully separated on GSiMe (Figure 4.19) were well resolved on GSiAc column. The enantioseparation of three dichlorostyrene oxides on both columns were compared in Figure 4.20. However, **25Me** and **34Me** could not be separated on GSiAc column. These aforementioned results suggested that the position and type of substituent on both analyte and cyclodextrin derivatives possess a major impact on enantioseparation. Unfortunately, not all six isomers of di-substituted styrene oxides are available to be investigated to reveal more meaningful information.

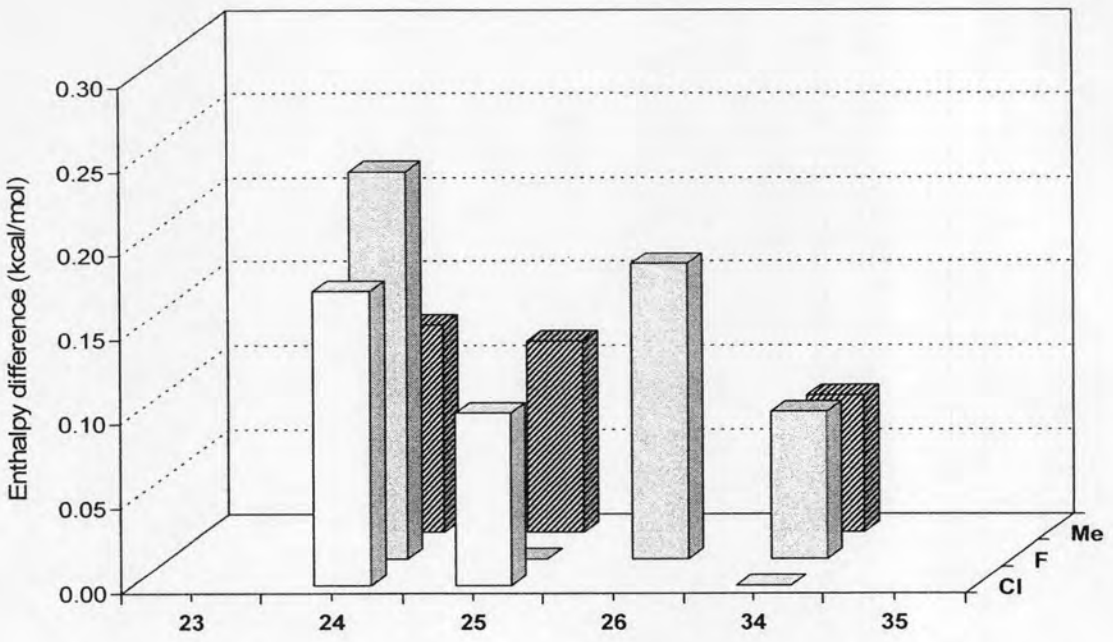

Figure 4.18 Enthalpy difference, $-\Delta\Delta H$ (kcal/mol) of the enantiomers of di-substituted styrene oxides on GSiMe column.

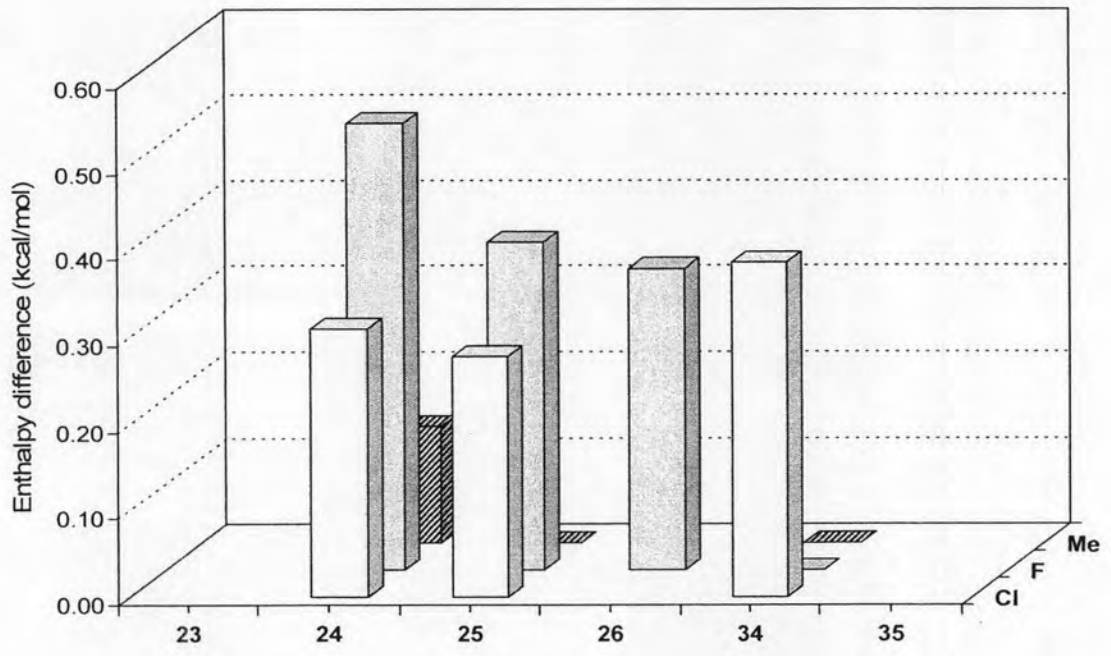

Figure 4.19 Enthalpy difference, $-\Delta\Delta H$ (kcal/mol) of the enantiomers of di-substituted styrene oxides on GSiAc column.

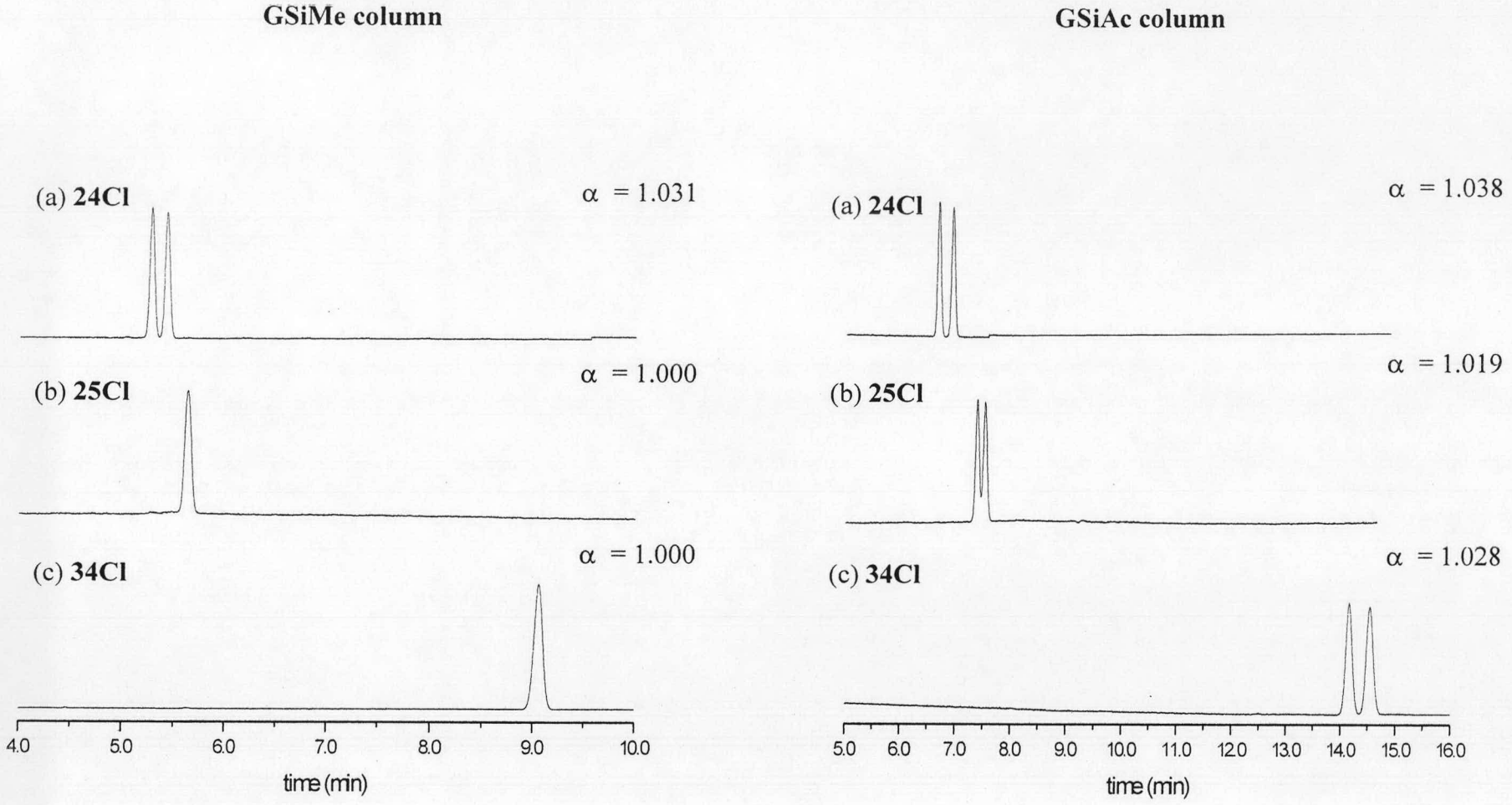

Figure 4.20 Chromatograms of (a) **24Cl**, (b) **25Cl**, and (c) **34Cl** on GSiMe (left) and GSiAc (right) columns at 120 °C.

Group 3: Other aromatic epoxides

Other aromatic epoxides with various types of substitution and structures were also investigated. The $-\Delta\Delta H$ values of aromatic epoxides in group 3 were compared to styrene oxide (**1**). For the simplicity of discussion, aromatic epoxides in group 3 are further divided into two subgroups.

Group 3.1: polyfluoro-substituted styrene oxides

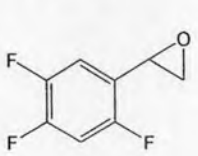

triF

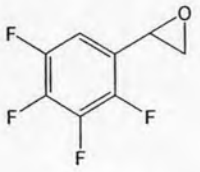

tetraF

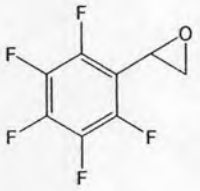

pentaF

Racemic epoxides in this subgroup comprise styrene oxide derivatives with trifluoro-, tetrafluoro-, and pentafluoro-substitution as shown above. The $-\Delta\Delta H$ values on GSiMe and GSiAc columns were compared with other monofluoro- and difluoro-substituted styrene oxides in Figure 4.21.

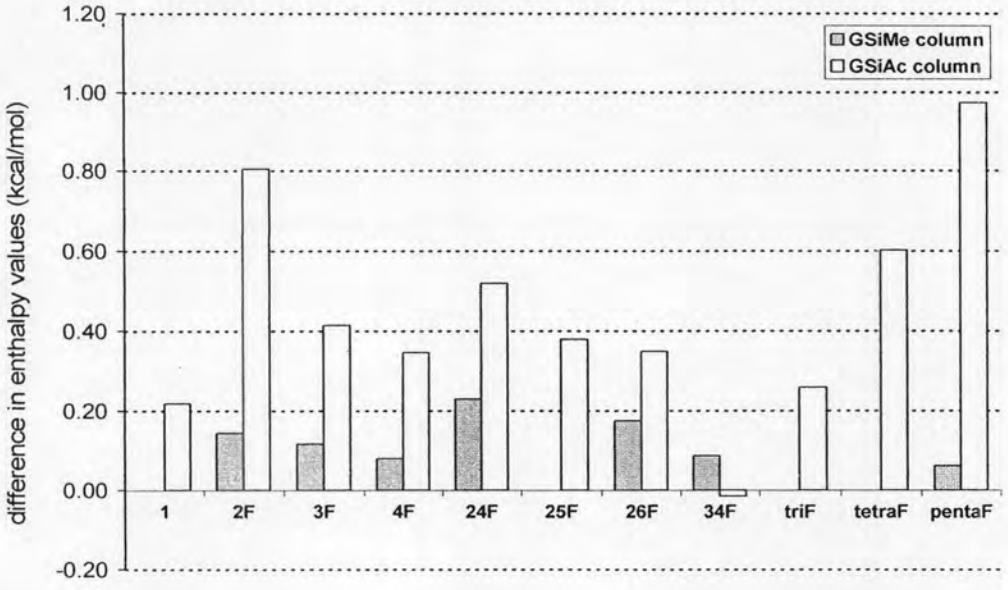

Figure 4.21 Enthalpy difference, $-\Delta\Delta H$ (kcal/mol) of the enantiomers of fluoro-substituted styrene oxides on GSiMe (gray bar) and on GSiAc (white bar) columns.

The $-\Delta\Delta H$ values of fluoro-substituted styrene oxides on GSiMe and GSiAc columns are substantially different. The $-\Delta\Delta H$ values of most analytes separated on GSiAc column were much larger than those obtained from GSiMe column, except for **34F**. While **25F**, **triF**, and **tetraF** were not resolved on GSiMe, all fluoro-substituted styrene oxides could be separated on GSiAc. The separations of **triF**, **tetraF,** and **pentaF** at 80 °C on both columns were compared in Figure 4.22. The enantioseparation of polyfluoro-substituted styrene oxides on GSiAc tend to improve with the number of fluoro-substitution. Among all fluoro-substituted epoxides, **pentaF** illustrated the best enantioseparation indicating that the effect of electronegative substituent towards enantioseparation on more polar GSiAc column. Unfortunately, other isomers of trifluoro- and tetrafluoro-substituted styrene oxides are not available to study the effect of position of fluoro-substitution.

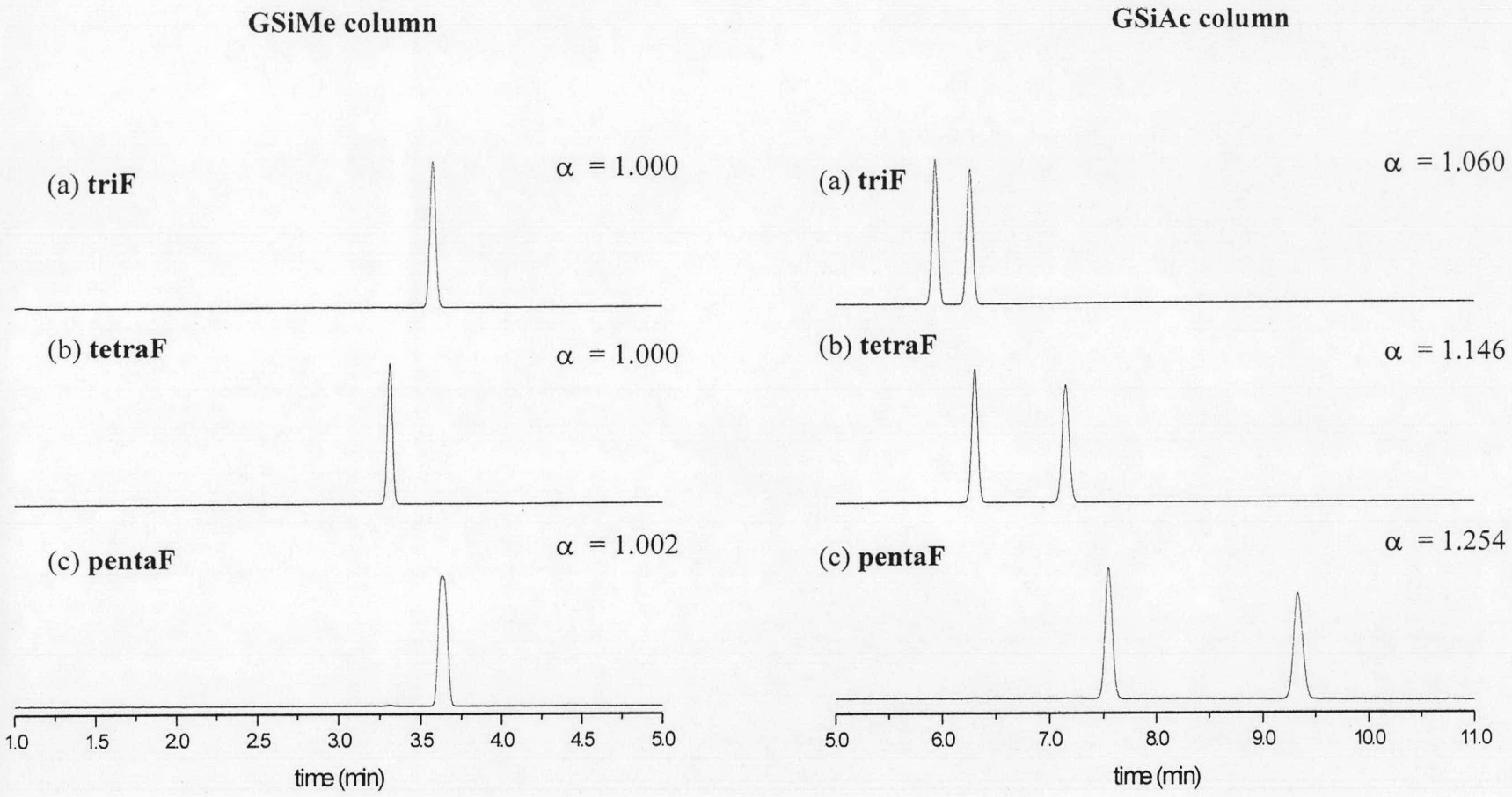

Figure 4.22 Chromatograms of (a) **triF** (b) **tetraF** and (c) **pentaF** on GSiMe (left) and GSiAc (right) columns at 80 °C.

Group 3.2: Aromatic epoxides with different structures

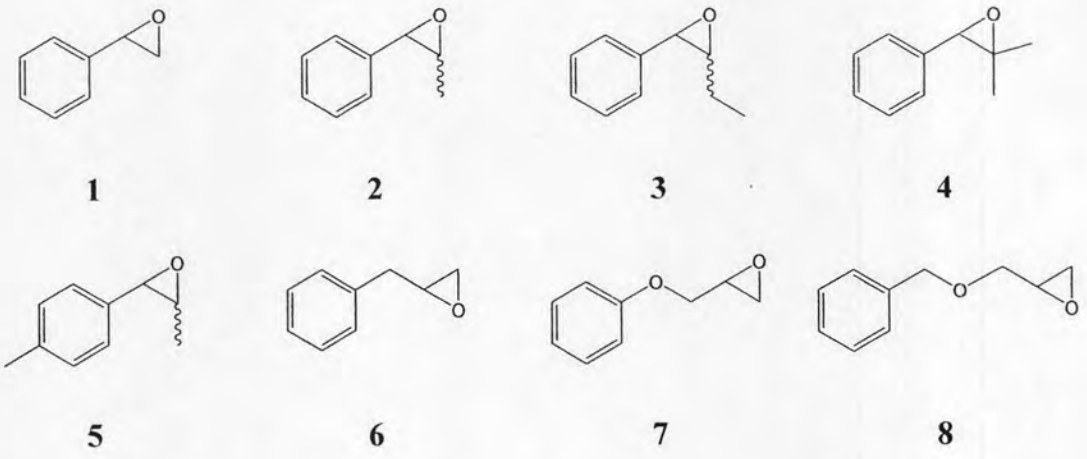

Epoxides in group 3.2 include derivatives of styrene oxide with different alkyl substitution on the side chain (as in **2**, **3**, **4** and **5**). Compounds **2**, **3**, and **5** are present in both *cis*- and *trans*-forms. Aromatic epoxides with different position of chiral center (as in **6**, **7** and **8**) are also incorporated. The $-\Delta\Delta H$ values of epoxides in group 3.2 on GSiMe and GSiAc columns were compared in Figure 4.23.

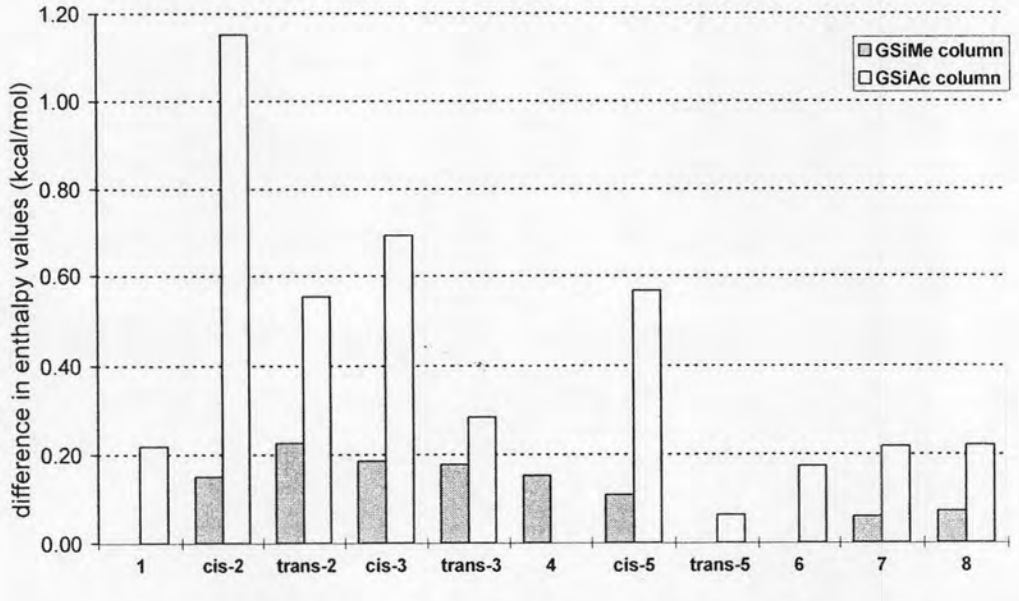

Figure 4.23 Enthalpy difference, $-\Delta\Delta H$ (kcal/mol) of the enantiomers of aromatic epoxides in group 3.2 on GSiMe (gray bar) and GSiAc (white bar) columns.

On GSiMe column, the enantioseparation of styrene oxide derivatives with different alkyl substitution on the side chain (**2, 3, 4,** and **5**) was better than that of styrene oxide (**1**), except for *trans*-**5** that showed no enantioseparation. However, geometric isomer (*cis*- or *trans*-) exhibited small or no influence towards enantioseparation as their $-\Delta\Delta H$ values were very similar (e.g. *cis*-**2** vs. *trans*-**2** or *cis*-**3** vs. *trans*-**3**). Comparing $-\Delta\Delta H$ values of analytes **1**, **6**, **7**, and **8** revealed that position of chiral center and introduction of oxygen atom into a side chain could influence enantioseparation. It can be seen that **1** and **6** could not be separated while **7** and **8**, having oxygen atom in the side chain, showed small resolution on GSiMe column (Figure 4.24). Nevertheless, the effect cannot be generalized from the results obtained in this study due to the limited number of analytes.

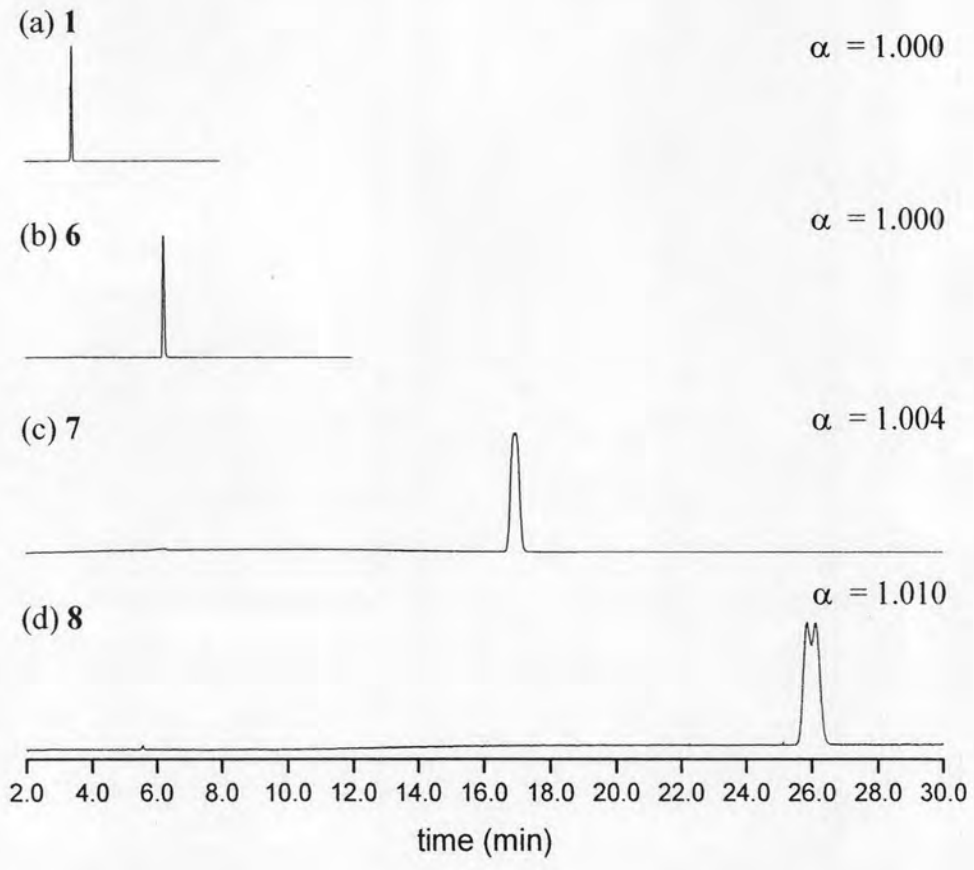

Figure 4.24 Chromatograms of (a) **1**, (b) **6**, (c) **7**, and (d) **8** on GSiMe column at 90 °C.

All enantiomers of analytes in group 3.2 could be separated on GSiAc column with higher $-\Delta\Delta H$ values, except for **4**. The effect of *cis*- and *trans*-isomers was clearly noticed since all *cis*-isomers of **2**, **3**, and **5** showed superior separation on GSiAc than their corresponding *trans*-isomers. Additionally, all *cis*- and *trans*-isomers of **2**, **3**, and **5** were better separated on GSiAc than on GSiMe. Figure 4.25 compares the separation of *cis*- and *trans*-isomers of **2**, **3**, and **5** at 90 °C on both columns. Interestingly, the effect of *cis*- and *trans*-isomers on GSiMe and GSiAc were opposite to results observed from BSiMe and BSiAc [16]. While BSiMe showed better enantioseparation towards *cis*-isomers, BSiAc exhibited similar enantioselectivity to both *cis*- and *trans*-isomers. Position of chiral center had very small influence on this column because **6**, **7**, and **8** gave similar $-\Delta\Delta H$ values and closed to that of styrene oxide (**1**).

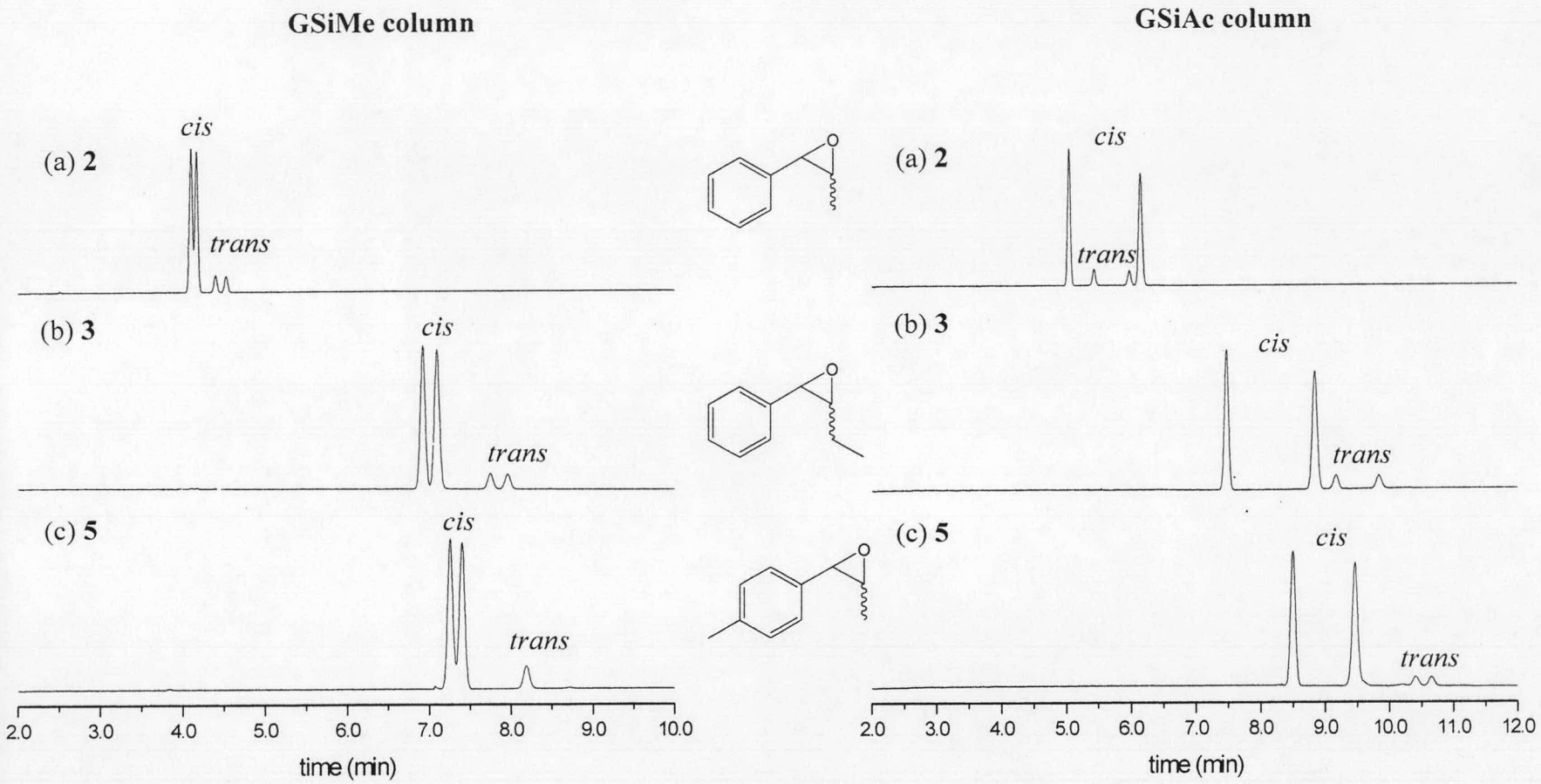

Figure 4.25 Chromatograms of (a) **2**, (b) **3**, and (c) **5** on GSiMe (left) and GSiAc (right) columns at 90 °C.

Group 4: Aliphatic epoxides

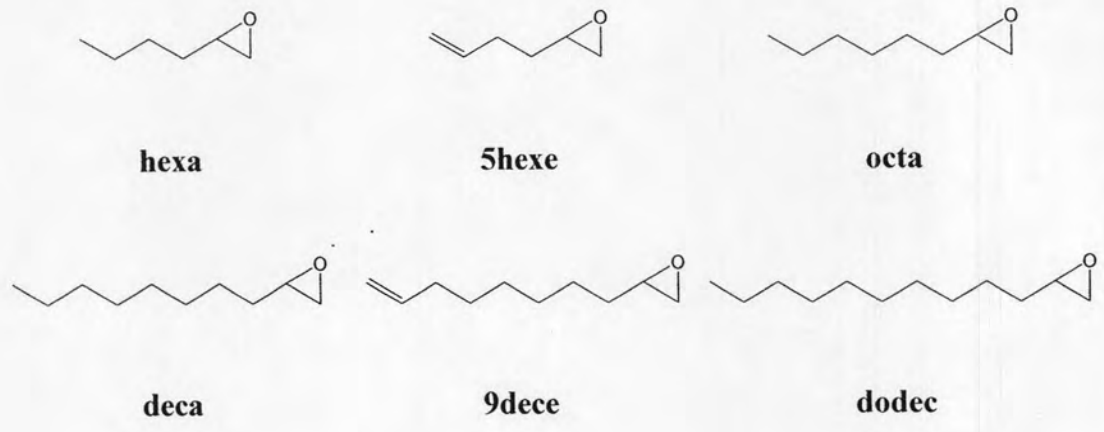

Epoxides in group 4 are aliphatic epoxides with different number of carbons (C_6–C_{12}), as shown above. The $-\Delta\Delta H$ values of epoxides in group 4 on GSiMe and GSiAc columns were compared in Figure 4.26.

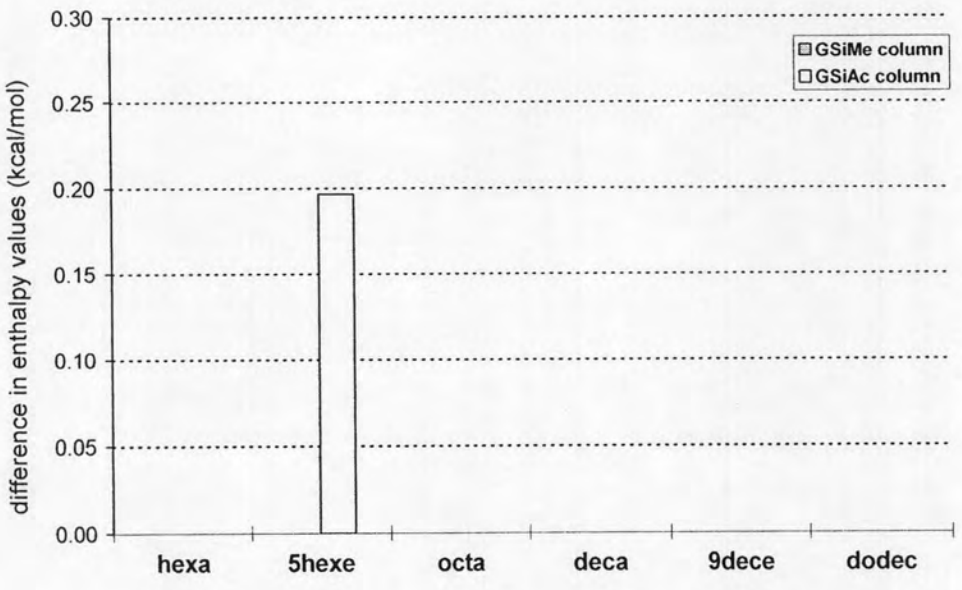

Figure 4.26 Enthalpy difference, $-\Delta\Delta H$ (kcal/mol) of the enantiomers of aliphatic epoxides on GSiMe (gray bar) and GSiAc (white bar) columns.

All epoxides in group 4 showed poor enantiodifferentiation on both GSiMe and GSiAc columns. While **hexa** could not be resolved, **5hexe** was the only analyte in this groups that could be separated on GSiAc column. This result indicated that a small modification in the analyte structure could greatly affect enantioseparation. It was evident that large-size cyclodextrin as GSiMe and GSiAc were not suitable for the enantioseparation of small and flexible aliphatic epoxides. Nevertheless, the effect cannot be generalized from the results obtained in this study.

Thermodynamic data obtained from GC experiment demonstrated the influence of analyte structure on enantioseparation. However, molecular modeling is still needed to understand the mechanism of chiral recognition between epoxides and CD derivatives. Among all epoxides studied, enantioseparation of group 1 mono-substituted styrene oxides on GSiAc column clearly indicated the influence of substitution position. Therefore, 18 styrene oxide derivatives with bromo, chloro, fluoro, methyl, trifluoromethyl and nitro substitution at *ortho-*, *meta-* and *para-* positions were selected as guests and GSiAc as host for investigation of the chiral recognition between analyte and chiral selector by molecular docking in this research.

4.3 Molecular modeling of the interaction between analyte and chiral selector

The docking results of the complexes between styrene oxide along with eighteen mono-substituted derivatives and GSiAc are presented for the dominating configuration with minimum binding free energy (ΔG) in Table 4.1. All enantiomeric complexes have a short span of binding free energy in the range −4.33 to −0.33 kcal/mol and a frequency range of 66−100%. Exceptions are the complexes of (*R*)-**4NO** and (*S*)-**4NO** that are least stable with binding free energies of 0.04 and 0.02 kcal/mol and frequencies of 94% and 50%, respectively. Consequently, the binding free energy differences of 0.00−0.28 kcal/mol are insignificant because they are about 10 times smaller than the standard error (~2.5 kcal/mol) of the docking calculations using AutoDock (Table 4.1). The ΔG values at 298 K between the selected analytes and GSiAc obtained from molecular docking (AutoDock 4) are also compared to those from GC. It was found that ΔG values at 298 K obtained from GC are in the range of −6.37 to −10.11 kcal/mol and are systematically larger than those obtained from molecular docking about 2−10 kcal/mol. Hence, for the molecular docking, the results are mainly discussed on the distinction in the inclusion geometries of the enantiomeric styrene oxides in the GSiAc cavity. The binding energy differences of the two enantiomeric complexes are further quantified by structure optimization of the dominating docked configurations with PM3 method.

Both (*R*)- and (*S*)-enantiomers of all analytes (guest molecules) are similarly embedded in the host GSiAc cavity. About 50% of the analytes situated at the GSiAc O2/O3 side align their long molecular axes parallel to the GSiAc plane. About 47% incline 45°/135° with respect to the GSiAc plane and point their epoxy groups towards the O2/O3 side (25%) and towards the O6 side (22%). The rest 3% align their long molecular axes perpendicular to the GSiAc plane. Effect of the substituent position on the inclusion geometry is shown for the three isomers of mono-substituted styrene oxide with trifluoromethyl- and nitro-groups (Figures 4.27 and 4.28). The (*R*)- and (*S*)-enantiomers of the *ortho*-substituted analyte are differently oriented in the GSiAc cavity, whereas those of the *meta*- and *para*-substituted analytes have similar orientation with epoxy group that always pointing in the same direction or flip 180 °.

Table 4.1 The binding free energies at 298 K between the selected analytes and GSiAc obtained from molecular docking (AutoDock 4) and GC.

Analyte		% frequency	$\Delta G_{AutoDock}$ [a] (kcal/mol)	$\Delta\Delta G_{AutoDock}$ [b] (kcal/mol)	ΔG_{GC} [c] (kcal/mol)	$\Delta\Delta G_{GC}$ [d] (kcal/mol)
1	*R*	100	–4.18	0	–6.79, –6.86	–0.07
	S	100	–4.18			
2Br	*R*	100	–4.33	–0.06	–7.54, –7.71	–0.17
	S	99	–4.27			
3Br	*R*	85	–2.36	–0.07	–7.98, –8.05	–0.06
	S	100	–2.29			
4Br	*R*	100	–3.35	–0.05	–8.01, –8.00	0.01
	S	99	–3.30			
2Cl	*R*	98	–3.91	–0.05	–7.20, –7.43	–0.23
	S	100	–3.86			
3Cl	*R*	100	–3.26	0.05	–7.59, –7.68	–0.09
	S	97	–3.31			
4Cl	*R*	86	–3.47	–0.01	–7.56, –7.58	–0.02
	S	68	–3.46			
2F	*R*	96	–1.25	0.28	–6.58, –6.84	–0.26
	S	100	–1.53			
3F	*R*	100	–2.63	–0.16	–6.81, –6.95	–0.14
	S	94	–2.47			
4F	*R*	84	–1.70	–0.03	–6.71, –6.83	–0.12
	S	100	–1.67			
2Me	*R*	100	–2.37	0.08	–7.21, –7.38	–0.03
	S	100	–2.45			
3Me	*R*	100	–0.38	–0.05	–7.25, –7.36	–0.06
	S	100	–0.33			
4Me	*R*	78	–1.80	0.02	–7.10, –7.12	–0.02
	S	97	–1.82			

Table 4.1 (continued)

Analyte		% frequency	$\Delta G_{AutoDock}$ [a] (kcal/mol)	$\Delta\Delta G_{AutoDock}$ [b] (kcal/mol)	ΔG_{GC} [c] (kcal/mol)	$\Delta\Delta G_{GC}$ [d] (kcal/mol)
2CF	*R*	100	–1.50	–0.24	–6.37, –6.63	–0.26
	S	81	–1.26			
3CF	*R*	66	–1.19	0.22	–6.99, –7.20	–0.21
	S	99	–1.41			
4CF	*R*	94	–1.27	–0.10	–6.96, –7.11	–0.15
	S	70	–1.17			
2NO	*R*	90	–2.26	0.11	–8.89, –9.18	–0.29
	S	99	–2.37			
3NO	*R*	74	–1.54	–0.08	–9.77, –9.77	0.00
	S	91	–1.46			
4NO	*R*	94	0.04	0.02	–9.89, –10.11	–0.22
	S	50	0.02			

[a] Minimum binding free energy obtained from AutoDock 4

[b] The binding free energy difference at 298 K between the (*R*) and (*S*) complexes, $\Delta\Delta G = \Delta G_R - \Delta G_S$; negative / positive value means the elution order *S* before *R* / *R* before *S* obtained from AutoDock 4

[c] The binding free energy at 298 K calculated from GC experiment between the less retained and more retained complexes, respectively

[d] The binding free energy difference at 298 K between the (*R*) and (*S*) complexes calculated from GC experiment

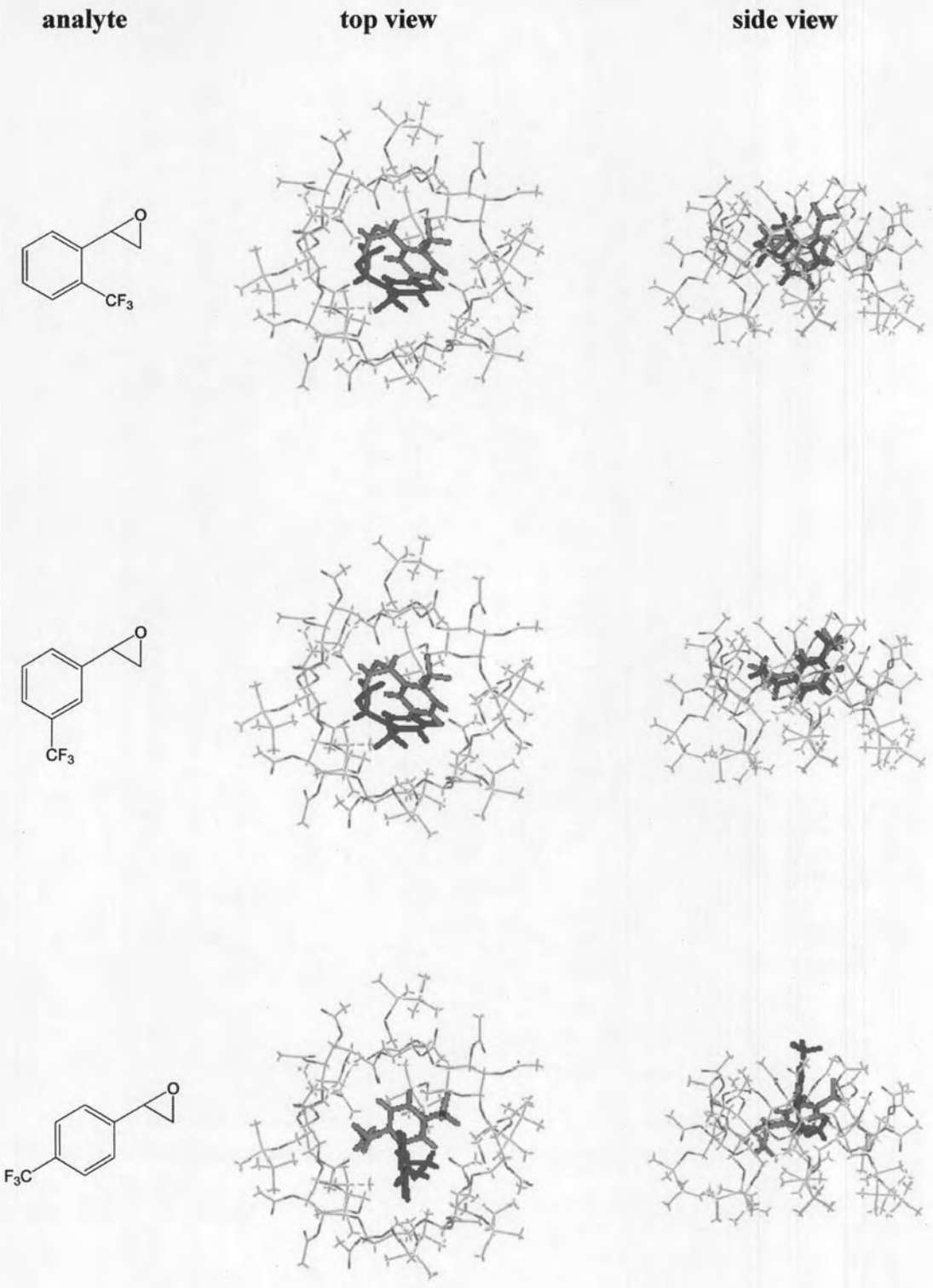

Figure 4.27 Superposition of the most stable complexes between GSiAc and (*R*)-enantiomer (green) and (*S*)-enantiomer (pink) of **2CF**, **3CF**, **4CF** in both top and side views.

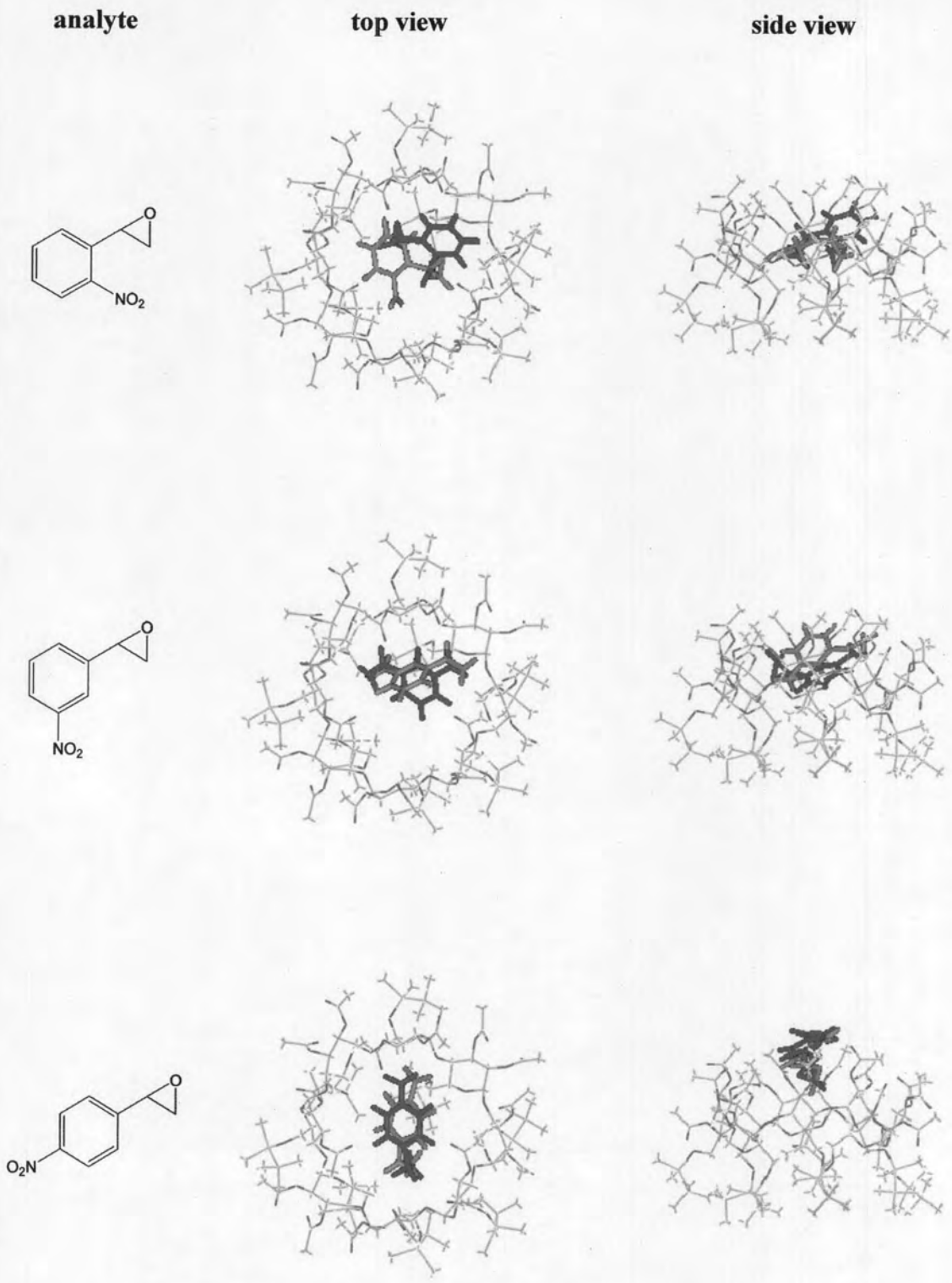

Figure 4.28 Superposition of the most stable complexes between GSiAc and (*R*)-enantiomer (green) and (*S*)-enantiomer (pink) of **2NO**, **3NO**, **4NO** in both top and side views.

Table 4.2 Formation energies of host and guest and binding energies of the complexes obtained from re-optimization with PM3 method.

Analyte		$E_{complex}$ (kcal/mol)	E_{guest} (kcal/mol)	$\Delta E_{binding}$ (kcal/mol)	$\Delta\Delta E^a$ (kcal/mol)
1	*R*	–2907.09	17.66	–11.18	–0.91
	S	–2906.18	17.66	–10.27	
2Br	*R*	–2893.66	26.15	–6.24	–2.21
	S	–2891.44	26.15	–4.03	
3Br	*R*	–2892.79	25.47	–4.70	0.42
	S	–2893.21	25.47	–5.12	
4Br	*R*	–2893.10	25.40	–4.94	1.29
	S	–2894.39	25.40	–6.23	
2Cl	*R*	–2909.18	11.89	–8.33	2.55
	S	–2911.73	11.89	–10.06	
3Cl	*R*	–2907.85	11.08	–6.80	–1.54
	S	–2906.31	11.08	–3.83	
4Cl	*R*	–2908.31	10.96	–5.70	–0.19
	S	–2909.18	10.96	–5.51	
2F	*R*	–2945.73	–25.09	–7.08	2.86
	S	–2948.59	–25.09	–9.93	
3F	*R*	–2945.03	–25.80	–5.67	–1.41
	S	–2943.62	–25.80	–4.26	
4F	*R*	–2946.56	–25.91	–7.08	1.51
	S	–2948.07	–25.91	–8.59	
2Me	*R*	–2914.03	17.66	–11.18	3.76
	S	–2917.80	17.66	–10.27	
3Me	*R*	–2914.04	26.15	–6.24	1.62
	S	–2915.66	26.15	–4.03	
4Me	*R*	–2916.28	25.47	–4.70	–1.27
	S	–2915.01	25.47	–5.12	

Table 4.2 (continued)

Analyte	$E_{complex}$ (kcal/mol)	E_{guest} (kcal/mol)	$\Delta E_{binding}$ (kcal/mol)	$\Delta\Delta E^a$ (kcal/mol)
2CF	–3059.04	–137.59	–7.88	–3.13
	–3055.91	–137.59	–4.75	
3CF	–3059.82	–140.59	–5.66	0.69
	–3060.50	–140.59	–6.35	
4CF	–3063.22	–140.53	–9.13	–0.44
	–3062.78	–140.53	–8.69	
2NO	–2911.88	12.06	–10.38	–2.66
	–2909.22	12.06	–7.72	
3NO	–2913.22	8.97	–8.63	–0.87
	–2912.35	8.97	–7.76	
4NO	–2911.75	9.07	–7.26	1.37
	–2913.12	9.07	–8.63	

* formation energy of host = –2913.56 kcal/mol

[a] The binding energy difference between the (*R*) and (*S*) complexes, $\Delta\Delta E = \Delta E_R - \Delta E_S$; negative / positive value means the elution order *S* before *R* / *R* before *S*.

Table 4.2 shows the binding energies of the complexes between the 18 enantiomeric mono-substituted styrene oxides and GSiAc derived from structure optimization with PM3 method. All enantiomeric complexes have binding free energy in the range of −11.18 to −3.83 kcal/mol. The GSiAc·(*S*)-**1** complex is less stable than the GSiAc·(*R*)-**1** complex as shown by the binding energies of –10.27 and –11.18 kcal/mol, respectively. The binding energy difference of the two enantiomeric complexes, ΔΔE, is –0.91 kcal/mol. This is consistent with the result obtained from GC showing that the (*S*)-**1** enantiomer is less bound to GSiAc and hence elutes before the (*R*)-**1** enantiomer. For the enantiomeric derivatives with different substituent positions, the enantiodifferentiation increases with increasing binding energy difference. The largest ΔΔE of the six complexes of the *ortho*-derivatives indicates their best separation on the GSiAc column when compared with the *meta*- and *para*-derivatives: –2.21, 2.55, 2.86, 3.76, –3.13 and –2.66 kcal/mol for the bromo-, chloro-, fluoro-, methyl-, trifluoromethyl- and nitro-derivatives, respectively (Table 4.2). The

binding energy differences of the chloro-, methyl- and trifluoromethyl- derivatives mentioned above are in order of *ortho-* > *meta-* > *para-*. Molecular modeling results are in good agreement with GC for the sequence of enantioseparation: *ortho-* > *meta-* > *para-*. In addition, the complexes of the nitrostyrene oxide with the binding energy difference in order *ortho-* > *para-* > *meta-* is also in agreement with the GC result. However, the binding energy difference of bromo- and fluoro-substituted styrene oxides in order *ortho-* > *para-*> *meta-* disagree with the GC results, *ortho-* > *meta-* > *para-*.

The results of molecular modeling obtained from this research were also compared to those from previous research. Most of analytes align at the wider rim and in the cavity of cyclodextrin derivatives which well agree with result obtained by Beier and Höltje [30]. Moreover, the binding energy difference of the two enantiomeric complexes ($\Delta\Delta E$) can be used to predict elution order in chiral separation on GC which less stable complexes are eluted before more stable complexes [30]. Nevertheless, the applicability of the procedure describes in this research still has to be proven by separation of many analytes which known their elution order.